

Carnegie Mellon University

CARNEGIE INSTITUTE OF TECHNOLOGY

DEPARTMENT OF BIOMEDICAL ENGINEERING

PROJECT REPORT

SUBMITTED IN PARTIAL FULFILLMENT OF THE REQUIREMENTS

FOR THE DEGREE OF Master of Science

TITLE The Hand Held Force Magnifier for Surgical Instruments

PRESENTED BY Randy Lee

ACCEPTED BY THE DEPARTMENT OF BIOMEDICAL ENGINEERING

George Stettin
FACULTY ADVISOR

5/14/2012
DATE

Carroll D. Rini
FACULTY READER

5/14/12
DATE

DEPARTMENT HEAD

DATE

The Hand-Held Force Magnifier for Surgical Instruments

Submitted in partial fulfillment of the requirements for
the degree of
Master of Science
in
Biomedical Engineering

Randy Lee

B.S., Bioengineering, University of California, San Diego

Department of Biomedical Engineering
Carnegie Mellon University
Pittsburgh, PA 15213

May, 2012

Copyright © 2012 Randy Lee
All rights reserved

Acknowledgements

Principally, I would like to thank my advisor, Professor George Stetten, for his generous mentorship and expertise in the day-to-day development of this project. This project would not have been possible without his patience and steady hand. I would also like to thank the VIA Lab, especially John Galeotti, Bobby Klatzky, Mel Siegel, Bing Wu, and Vikas Shivaprabhu for their valuable input throughout the design process. Finally, I dedicate this manuscript to my parents, for instilling in me the drive to continuously strive for the highest heights.

Abstract

In the modern era of surgery, clinicians often find that they must sacrifice their sense of touch in favor of microsurgical or minimally invasive approaches. We present here the Hand Held Force Magnifier (HHFM), a novel surgical tool which is able to measure tissue forces at the tool tip and apply amplified forces to a user's hand. The resulting effect is that tissue properties are magnified, augmenting a clinician's abilities in the surgical suite. Two successive generations of the HHFM have been built and characterized. Preliminary psychophysical experiments have shown that absolute force perception thresholds are reduced with the HHFM, and that differential force perception is improved. Additional psychophysical experiments are currently underway to better characterize user behavior following membrane puncture. Work has also been done to evaluate the market potential for an HHFM surgical tool.

Table of Contents

Acknowledgements	i
Abstract	ii
List of Figures and Illustrations	v
List of Acronyms and Symbols Used	vi
1 Introduction	1
1.1 Motivation: Emergence of the “Haptic” Problem.....	1
1.2 Overview	3
1.3 Thesis Outline.....	4
2 Literature Review	5
2.1 Mechanisms and Errors in Force Measurement.....	5
2.1.1 Hookean Force Measurement	5
2.1.2 Resistive Force Measurement.....	6
2.1.3 Piezoelectric Force Measurement	7
2.1.4 Measurement Errors.....	7
2.2 Existing Technology.....	8
2.2.1 Micron	8
2.2.2 MicroTactus	9
2.2.3 The Steady Hand Robot	10
2.2.4 The da Vinci and Pneumatic Array Feedback.....	11
3 The Model-1 Hand-Held Force Magnifier	13
3.1 Model-1 Development.....	13
3.1.1 Prototype Construction.....	13
3.1.2 Electronics and Control System	14
3.2 Model-1 Psychophysical Experiments	14
3.3 Model-1 Discussion	16
4 The Model-2 Hand-Held Force Magnifier	17
4.1 Model-2 Development.....	17
4.1.1 Brace and Actuator Assembly	17

4.1.2 Hydraulic Pressure Sensor Prototype	18
4.1.3 Guidewire Pressure Sensor Prototype	20
4.1.4 Magnetically Stabilized Prototype	22
4.1.5 Leaf Spring Preload Prototype	27
4.1.6 Shim Stock Preload Prototype	28
4.1.7 Electronics and Control Systems	29
4.2 Model-2 Psychophysical Experiments	34
4.3 Model-2 Discussion	35
5 Future Work and Conclusion	36
5.1 Model-3 and Beyond.....	36
5.2 A Commercial Future for the HHFM	37
5.2.1 The Unmet Clinical Need and Market Size.....	37
5.2.2 Emergent Engineering Challenges	38
5.2.3 Intellectual Property and Patent Landscape	39
5.2.4 Proposed Business Model	40
5.3 Conclusion.....	42
References	44
Appendix A.....	47
Model-1 Electronics	48
Appendix B.....	49
Model-2 Electronics	50
Model-2 Control Code (LabVIEW).....	51
Model-2 Control Code (Analog Devices).....	53

List of Figures and Illustrations

Figure 1-1. Minimally invasive surgery set up

Figure 1-2. Hand-Held Force Magnifier concept

Figure 2-1. The Wheatstone Bridge

Figure 2-2. The *SteadyHand* eye robot

Figure 2-3. Evolution of the *Steady Hand* force sensor

Figure 3-1. The Model-1 HHFM

Figure 3-2. Model-1 psychophysical experiments results

Figure 4-1. Digital prototype of Model-2 brace and actuator assembly

Figure 4-2. Hydraulic pressure sensor prototype

Figure 4-3. Guidewire pressure sensor schematic

Figure 4-4. Guidewire pressure sensor prototypes

Figure 4-5. Guidewire pressure sensor loading curves

Figure 4-6. Magnetically stabilized prototype design schematics

Figure 4-7. Magnetically stabilized force sensing assembly

Figure 4-8. Raw sensor voltage and coil voltage in magnetically stabilized prototype

Figure 4-9. Digital prototype of leaf spring prototype

Figure 4-10. Shim stock prototype

Figure 4-11. Front panel to Model-2 electronics enclosure

Figure 4-12. NI DAQ noise variation within operating systems

Figure 4-13. NI DAQ sampling period variation within operating systems

Figure 4-14. Model-2 knob-controlled gain vs. hardcoded gain

Figure 4-15. MLHD interface with dummy handle.

Figure 5-1. Proposed Model-3 with surface mount force sensors

Figure 5-2. Patent publishing trends in haptic technology

List of Acronyms and Symbols Used

A/D – Analog-to-Digital

CPU – Central Processing Unit

D/A – Digital-to-Analog

DAQ – Data Acquisition Unit

DoF – Degrees of Freedom

GUI – Graphical User Interface

HHFM – Hand-Held Force Magnifier

I/O – Input/Output

ILM – Inner Limiting Membrane

MIS – Minimally Invasive Surgery

MLHD – Magnetically Levitated Haptic Device

NI – National Instruments

OS – Operating System

RCoM – Remote Center of Motion

SHR—Steady Hand Robot

VI – Virtual Instrument

f – force, in units N

k – Hookean stiffness constant, in units N/m

ε – Engineering Strain, unitless

σ – Engineering Stress, in units N/m² or Pa

ρ – resistivity, in units Ω -m

κ – dielectric constant, unitless

ε_0 – the permittivity constant, value of $8.8542 \times 10^{-12} \text{ C}^2/\text{Nm}^2$

1 Introduction

1.1 Motivation: Emergence of the “Haptic” Problem

The art and science of surgical intervention have advanced tremendously since its emergence as an offshoot from the field of medicine beginning in the 1800’s [1]. Advances in sterile technique, anesthetics, analgesics, and surgical instrument design have pushed the surgeon from a simple bone-setter and to a respected medical specialist. Initially, large incisions into the body were made to expose the patient’s tissues and organs, giving the surgeon a relatively large workspace and direct line of sight as they worked. In this way, an extensive compendium of procedures was developed and refined by successive generations of dedicated specialists. Yet, the risk of infection and complications, the need for long recovery times, and cosmetically unappealing scarring have all been reasons to pursue less drastic approaches. Most notable in the modern era of medicine (mid-1900’s to 2000’s) is the development of minimally invasive and microsurgical procedures.

Minimally invasive surgery (MIS) is a subspecialty of general surgery that all but eliminates the need for surgeons to make large incisions into the body. Access to an internal cavity is achieved through several ports in the body, through which cameras, lights, and surgical tools are inserted. An inert gas (e.g. CO₂) can also be used to inflate the cavity and increase the surgeon’s working space [2]. **Figure 1-1** shows a typical MIS set up. Minimally invasive approaches have been associated with reduced postoperative pain, reduced postoperative infection, and shorter periods of disability [3-5]. However, this approach to surgery still presents significant challenges. Operating through instrumented ports drastically reduces the clinician’s workspace and field of view, and almost always eliminates a surgeon’s sense of depth because only one camera is inserted into the body to provide visual feedback. Surgical

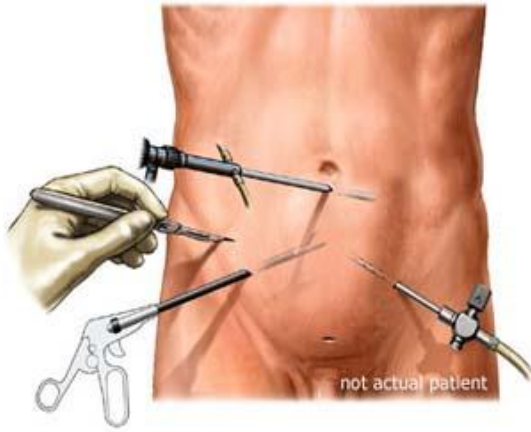


Figure 1-1. Minimally invasive surgery [6].

tools must be specially designed to accommodate for these new constraints. MIS tools are commonly actuated like scissors, and feature long bodies to allow for tool insertion. A significant problem associated with these designs is that mechanical torques and frictional forces are generated between the tool and the point of entry, confounding the tactile feedback perceived by the clinician. Further, physiological tremor and unintended movements are magnified through a lever arm effect. Yet through all of these challenges, specialists have been able to develop a number of minimally invasive

procedures that promise to improve patient outcomes. Common minimally invasive procedures include orthopaedic surgeries like knee replacement and anterior cruciate ligament repair, *radical prostatectomies* and *vasectomies* in urology, and *cholecystectomies* (gallbladder removal) and *gastrectomies* (stomach removal) in abdominal surgery.

Alongside MIS, microsurgical approaches have developed in recent years as a subspecialty of general surgery. In microsurgery, clinicians may still make incisions to directly access tissues of interest, but in general they operate on relatively small structures like the peripheral nerves and vessels, or thin basement membranes. Retinal surgery, for example, was a frontier previously untouched in the development of general surgical practice. One common procedure in the retina is the removal of the inner limiting membrane (ILM), a basement membrane of the retina. In a diseased state called macular pucker, the ILM clouds a patient's vision and its removal has been associated with improvements to visual acuity [7]. In a related condition, called macular hole, removal of the ILM has also been shown to improve visual acuity [8]. In model organisms (chick and rat), the mature ILM has an average thickness of only 400 μm , which makes procedures difficult because the internal forces generated by pulling on this tissue fall far below the threshold of human perception [9]. Gupta and colleagues have directly measured tissue forces during retinal microsurgery, and found that up to 75% of all tissue interactions yield forces lower than 7.5 mN, and were perceived by the surgeon only 19% of the time [10]. To work with these extremely delicate tissues, specialty tools and techniques have been developed to help compensate for challenges unique to the practice. In the total absence of tactile feedback, for example, retinal microsurgeons have been trained to rely on visual feedback alone. Microsurgical techniques are common in vascular surgery, plastic and reconstructive surgery, and neurosurgery.

Novel surgical tools and techniques continue to be developed. The miniaturization of computing resources and mechanical components has allowed for the introduction of high technology in the operating theatre and the advent of robot-assisted surgeries. These technologies provide the surgeon with information crucial to the success of a procedure, or with abilities not possible with non-instrumented tools. For example, the *da Vinci* surgical system (Intuitive Surgical, Inc., Sunnyvale, CA) allows surgeons to minimally invasively operate on a patient from a console separated from the operating table, controlling up to three independent arms at once. Because the movement of robotic arms is more precise and repeatable than typical physiological movements, the *da Vinci* is able to reduce tremor and scale motion to the preference of the clinician. Advanced design of the attached MIS tools allows for wrist-like movements and degrees of freedom not seen in other systems.

Yet we have seen, in the advancement of technology and surgical technique alike, that the sense of touch is often sacrificed at these new surgical frontiers. We call this loss of tactile sense, which is characteristic of minimally invasive or microsurgical procedures, a “haptic” problem. It is one that concerns the sense of touch. A technology that could improve on, or return completely, the sense of touch would return these new types of surgery closer to the original sensory experience of traditional open surgery. In the present thesis, we describe the Hand Held Force Magnifier (HHFM), a novel surgical tool which aims to return the sense of touch to a clinician during procedures where haptic feedback is reduced or completely absent.

1.2 Overview

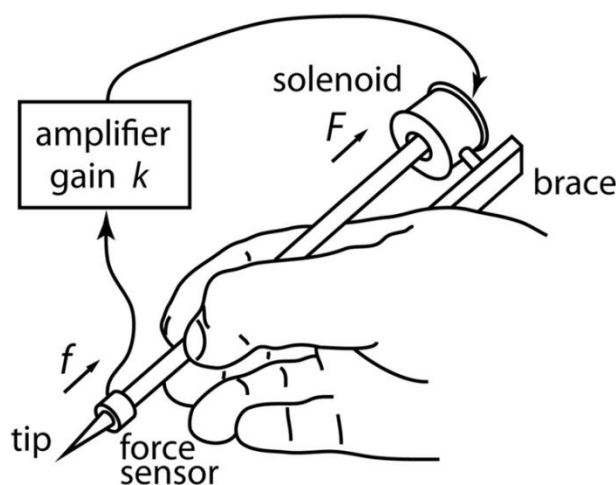


Figure 1-2. Schematic of the HHFM concept [11].

The HHFM is shown in a conceptual form in **Figure 1-2**. A sensor measures the reaction force, f , generated by tissue as the clinician works. The measurement is conditioned, amplified, and fed directly to an actuator. The actuator generates an amplified force, F , between the actuator and the clinician’s fingers, providing in essence a magnification of the tissue properties. Delicate tissues, for example, will feel stiffer. Critical events, such as tissue tearing, may become easier to detect. Careful investigation of the physical

limits of the device, as well as the perceptual limits of the human user, will be essential to the long-term efficacy and safety of the technology as a surgical tool.

1.3 Thesis Outline

This thesis begins with an overview of the surgical motivations for this project, and continues with a literature review of the existing technology. Although the field of robot-assisted surgery is still in its infancy, many lessons may be learned from the study of initial attempts towards a high tech operating room. Next, we describe the development of Model-1 and Model-2 of the HHFM. The Model-1 is a unidirectional proof of concept, while the Model-2 is a bidirectional prototype that refines device design and performance. Psychophysical studies using both Model-1 and Model-2 are also discussed. Finally, design lessons, psychophysical guidelines, and proposals for future work are made.

2 Literature Review

2.1 Mechanisms and Errors in Force Measurement

A major constraint in the design of instrumented surgical tools is the limited number of sensing modalities available to the engineer. Two goals paramount in measurement science are repeatability and predictability, qualities that are often marred by the properties of real materials in an imperfect world. The accurate and reproducible measurement of force is essential to the operation of the HHFM. While there are a multitude of theoretically possible force measurement methodologies, we focus here on the most common and simplest mechanisms.

2.1.1 Hookean Force Measurement

Hooke's law for ideal springs describes the force generated by a spring for a particular displacement. **Equation 1** describes this well-known relationship,

$$f = kx \quad (\text{Eq. 1})$$

where k is the spring constant, a measure of the stiffness of the spring, and x is the length of the spring [12]. The force f can be signed, differentiating tensile forces from compressive forces. Assuming we know *a priori* the k constant for a given spring, force measurement reduces to a length or distance measurement. Capacitive, optical, and electromagnetic position sensors can all be highly accurate, high-resolution methodologies for position measurement.

Expansion of **Equation 1** to three dimensions can be achieved by extending the relationship to

$$\sigma = C\varepsilon \quad (\text{Eq. 2})$$

where C is the 4th order stiffness tensor; σ is the stress, the applied force divided by cross-sectional area; and ϵ is the strain, the ratio of deformed length to original length. While bulk material force sensors may be possible in principle, in practice they can be difficult to use accurately and reliably because the stiffness tensor C can be difficult to obtain either analytically or experimentally to a suitable precision.

2.1.2 Resistive Force Measurement

Resistive approaches to force measurement rely on changes in the resistance of a wire in response to material strain. As such, these devices are often called strain gages. The following relationship between resistance R and wire length L can be written as

$$R = \frac{\rho L}{A} \quad (\text{Eq. 3})$$

where A is the cross sectional area of the wire and ρ is the resistivity, in units ohms-meters [13]. Error analysis of **Equation 3** shows a high dependence of resistance on the physical characteristics of the wire

$$dR = \left(\frac{L}{A}\right) d\rho + \left(\frac{\rho}{A}\right) dL - \left(\frac{\rho L}{A^2}\right) dA \quad (\text{Eq. 4})$$

As such, we see that single strain gages can be very sensitive to thermal expansion and contraction of the wire. Most strain gages, however, are manufactured in serpentine arrangements, so that changes in length (indicative of strain in a particular direction) dominate the change in resistance. Further, by installing the gages as part of a Wheatstone bridge, measurements independent of temperature can be made. **Figure 2-1** shows this common configuration, where R_x denotes the strain gage. At the point of

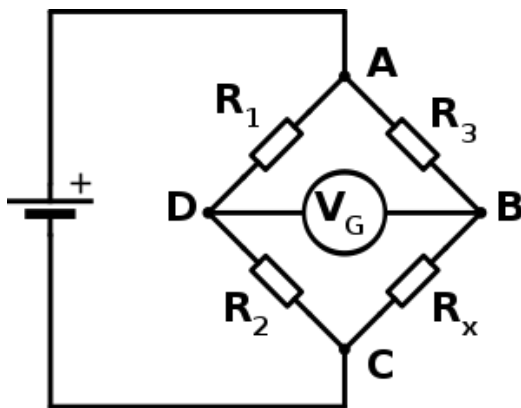


Figure 2-1. The Wheatstone bridge. [37]

balance, $R_1 = R_2 = R_3 = R_x$ and the following ratios are equivalent by Kirchhoff's Laws

$$\frac{R_2}{R_1} = \frac{R_x}{R_3}$$

But rather than measure the change in resistance directly, measurements of force using resistive measures usually reduce to measuring changes in an output voltage. In the Wheatstone bridge, when the strain gage is loaded, the resistance of R_x changes, which in turn creates a voltage across terminals B and D.

2.1.3 Piezoelectric Force Measurement

The piezoelectric effect is a phenomenon characterized by the generation of an electric field with strain in a crystalline material. The most common piezoelectric materials are quartz (SiO_2) and the polymer polyvinylidene fluoride (PVDF). The piezoelectric effect originates from an uneven distribution of charge due to strain in the crystalline lattice. Piezoelectric sensors are often assembled by placing electrodes across the material, forming a capacitor system with the crystal between the electrodes. The relationship between charge and force for a piezoelectric material can be given as

$$Q_x = d_{11} F_x \quad (\text{Eq. 5})$$

where Q_x is the charge generated due to force in the x direction, d_{11} is the piezoelectric coefficient in the direction of the applied force and orthogonal to its face, and F_x is the applied force [12]. Therefore, the voltage generated by the piezoelectric system as a capacitor is given by

$$\begin{aligned} V &= \frac{Q_x}{C} = \frac{d_{11}}{C} F_x \\ &= \frac{d_{11}L}{\kappa \epsilon_0 a} F_x \end{aligned}$$

where κ is the dielectric constant of the crystal, ϵ_0 is the permittivity constant ($8.8542 \times 10^{-12} \text{ C}^2/\text{Nm}^2$), L is the distance between the plates, and a is the area of the electrodes. Piezoresistive force sensing uses the piezoelectric effect to change the resistance in a sensing element.

The piezoelectric phenomenon is reversible. An applied voltage across a piezoelectric material results in a physical deformation. Some devices, like the Squiggle motor (Newscale Technologies, Victor, NY), utilize this reverse relationship to actuate motion [14]. Piezoelectric force sensors are typified by small displacements and an inability to sustain a signal with static forces. This latter problem is particularly troublesome in our application, and led us to choose the strain gauge instead.

2.1.4 Measurement Errors

An important aspect of modern device design is signal conversion from the analog domain to the digital space, and vice versa. While digital signals may be easily analyzed and stored with computers, they are quantized and only represent a certain level of resolution. Analog signals, on the other hand, follow well-known principles and relationships, but are subject to electromagnetic interference and signal loss characteristic of real-world materials. The terminology surrounding common types of measurement errors has been largely standardized in engineering practice. This short glossary describes the most common definitions of measurement errors. Fraden has published an excellent text on this topic [12].

Hysteresis—a hysteresis error is the deviation in sensor output at a specified input when approached from opposite directions. For example, increasing a load to a specific point will yield an output voltage different from one obtained by decreasing the load to that same point. Hysteresis is commonly described to as “path dependency.”

Drift—drift describes the short- and long-term stability of a signal. Short-term drift can be bi-directional, and changes over time scales of minutes, hours, or days. Long-term drift arises from the aging of sensor materials, and is usually unidirectional.

Noise—noise is the stochastic disturbance of a signal that it is largely irregular and unpredictable. There are many different types of noise, including Johnson noise, which arises due to the quantum nature of electric current and thermal variations; shot noise, the well-known “white noise” that increases in magnitude with bias current in DC circuits; and pink noise, which is prevalent at lower frequencies because of greater correlation over time.

2.2 Existing Technology

Numerous technologies are currently under development to approach the problem of reduced haptic feedback during surgical procedures. Telerobotic systems, in which the clinician controls a slave robot at the patient’s bedside from a master terminal, are popular research topics, but only Intuitive’s *da Vinci* has advanced sufficiently to be commercially available for clinical use. Vibrotactile, cooperative, and pneumatic force feedback systems are discussed in this section, and represent the state-of-the-art in experimental technologies that attempt to address the haptic problem.

2.2.1 *Micron*

Micron is a device developed by the Surgical Mechatronics Laboratory at Carnegie Mellon University (Pittsburgh, PA) that aims to reduce physiological tremor during microsurgical procedures [15]. Although force feedback is not the primary goal of the *Micron* project, it is included in this literature review because *Micron* is one of the first experimental devices to address the small workspace and the demanding sensor requirements characteristic of retinal microsurgery. The device is completely hand-held, and utilizes three piezoelectric actuators to drive movement of a tool tip in three Degrees of Freedom (DoF) independent from motion of its handle. Optical tracking is used to obtain handle pose information to a sensitivity of 4 μm , while a closed-loop feedback algorithm and specialized tremor filters are implemented to minimize position error in real-time. The piezoelectric actuators are capable

of producing up to 1 N of force, more than required to resist and compensate for tool tip deflections originating from tremor. The range of motion achieved by the piezoelectric actuators is approximately 1 x 1 x 0.5 mm, centered on the handle [16]. Other iterations of the *Micron* device have a range of motion up to 3 x 3 x 0.8 mm [17].

Characterization experiments have shown efficacy of the system in filtering unwanted movements from those that are intentional [15]. Simple micromanipulation tasks with *Micron* include holding a stationary position, tracing a 500 μm diameter circle, and moving from one point to another 500 μm away. Recently, *Micron* has been used successfully in *ex vivo* vessel cannulation tasks, and some preliminary work has been done with *Micron* in membrane peeling tasks [16,17]. These simulated surgical tasks were done under a stereomicroscope and control was accomplished with vision-based methods. While the goal of *Micron* is not to provide force feedback to the user, control over unintentionally applied forces is improved when using *Micron* for microsurgical tasks. In effect, *Micron* accomplishes a different goal to that of the HHFM, although with somewhat similar means.

2.2.2 *MicroTactus*

MicroTactus is an instrumented, hand-held probe developed by the Haptics Laboratory at McGill University (Montreal, Canada). The goal of the project is to enhance tactile sensitivity during minimally invasive surgical tasks like tissue probing and exploration [18]. During minimally invasive knee surgery, for example, a surgeon may explore cartilaginous tissues with a tool to identify anomalies in the tissue. Haptic feedback in this task is confounded because of the moments and frictional forces generated while operating through MIS tool ports. In *MicroTactus*, a 90-degree bent arthroscopic tool was instrumented with an accelerometer to identify structure and texture on a surface. The tool was also fitted with a suspended rare-earth magnet to inertially actuate vibrotactile stimulation. The accelerometer was oriented orthogonal to the actuator to decouple the input signal from the device output. The system is also capable of delivering auditory feedback.

Psychophysical experiments showed that tactile or auditory feedback improved user performance in surface feature detection tasks, namely the identification of cuts in an otherwise smooth pad. Deep cuts were able to be identified both with and without feedback, while the identification of shallow cuts was improved among users with either tactile or auditory feedback. There was no significant difference in user performance between the two feedback mechanisms.

While the *MicroTactus* project does not offer the same kind of force feedback as pursued in the HHFM, we may still derive some important design lessons from the work. For example, it was seen that

the response of the device was somewhat dependent on the user's grip. Relaxed grips could potentially act as low-pass filters, with the finger tissue absorbing high frequency vibrations with the device in operation. To further guide haptic design, Lederman and Klatzky described the effect of probe size, exploration speed, and other variables in [19]. Furthermore, the orthogonal configuration between sensor and actuator minimized mechanical feedback. Yet, physiological tremor in one direction could still be unintentionally amplified, driving the actuator and yielding false positives.

2.2.3 The Steady Hand Robot

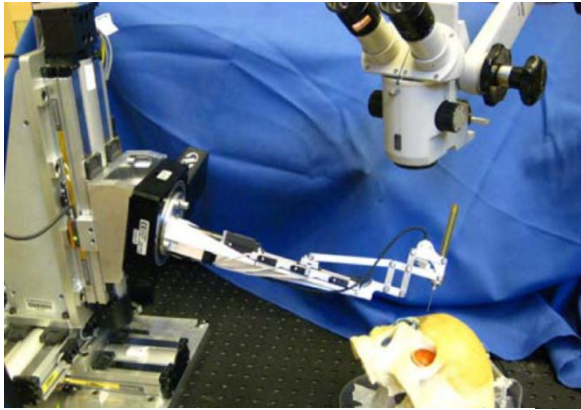


Figure 2-2. The Steady Hand Robot 2. [20]

The *Steady Hand Robot* (SHR) is a cooperative robot for vitreoretinal surgery developed at the Engineering Research Center for Computer-Integrated Surgical Systems and Technology at Johns Hopkins University (Baltimore, MD) [20,21]. The SHR is classified a “cooperative” robot because both machine and surgeon share control over an instrumented tool as it interacts with tissue. Sensors in the remote center of motion (RCoM) arm and in the tool detect user actions and limit arm velocity such

that global safety limits are respected. The most recent iteration, the SHR2, is shown in **Figure 2-2**.

Of particular interest in this project is the methodology of force measurement. In the SHR1, the force sensor was a micro-machined structure, consisting of concentric cylinders supporting a long tool tip [22]. Radial beams established contact between the outer cylinder and the tool tip, and strain gages were attached to the beams. Bending of the tool tip due to tissue interaction resulted in bending of the beams, from which the tissue force can be obtained. The force sensor in the SHR1 is able to measure forces up to 1 N in magnitude, with 0.25 mN resolution. The gages are arranged in a half-bridge configuration to reduce thermal variation and improve signal to noise ratio. A total of 8 gages are used in the configuration shown in **Figure 2-3a**. With the SHR2, the strain gage configuration was abandoned in favor of an optical force sensor [23]. In this configuration, strain at the tool tip produces a change in the characteristic Bragg wavelength, due to index change or grating pitch change in the optical fiber. This design is shown in **Figure 2-3b**. Calibration of the system shows that the design meets the 0.25 mN force resolution goal. A 2 DoF design of the fiber Bragg sensor is achieved by integrating three fiber Bragg grating fibers into a single titanium wire [23].

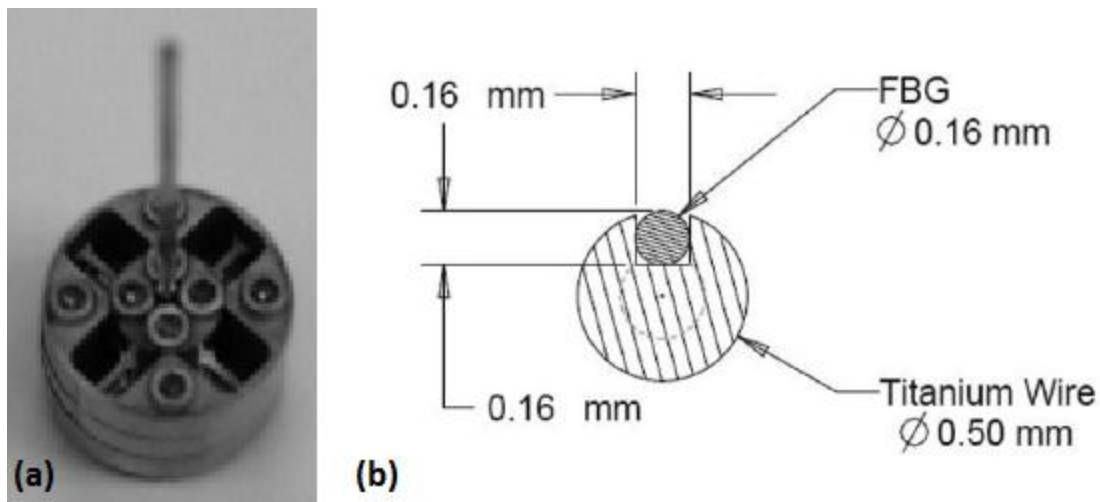


Figure 2-3. Force sensor assembly designs from (a) Steady Hand Robot 1 and (b) Steady Hand Robot 2. [22,23]

The SHR1 and SHR2 have contributed considerable insight into the requirements necessary for a surgical robot for retinal surgery, but a number of challenges must be met before the device can be integrated into the clinic. The large size of the robot, with its numerous stages and complex RCoM mechanism, make it undesirable in the already crowded operating theatre. Furthermore, the large forces required to actuate movements in the shared arm make surgeon fatigue a serious issue. Finally, it is unclear how the entire robot could be sterilized and re-used in the clinical setting.

2.2.4 The *da Vinci* and Pneumatic Array Feedback

Another technology that attempts to address the haptic problem is a pneumatic force feedback system developed at the Center for Advanced Surgical and Interventional Technology (CAISIT) at the University of California, Los Angeles. The system is integrated into the *da Vinci* telesurgical robot, presently the only commercially successful robotic system for minimally invasive surgery.

The *da Vinci* system consists of two stations: the master control console, and the robotic slave. The surgeon sits at the master console and manipulates two rotating control arms with their thumb and index finger. At the patient's bedside, separated from the console, the surgeon's hand motions are translated into motions in two robotic arms fitted with specialty MIS tools. Movement of the tools is accomplished with a high fidelity, high DoF actuator called *EndoWrist*, which uses a system of gears and pulleys to actuate tool use in the minimal space available in MIS. In this way, the surgeon is able to perform dexterous, natural movements in the constrained workspace of the body. Cameras and lights at the end of a third tool capture video of the operating field, which is presented to the surgeon at the console stereoscopically, restoring some sense of depth.

The *da Vinci* system is called "telesurgical" because the console is physically separated from the patient's bedside. Of course, this also means that the haptic problem is all the more pressing. *Da Vinci*

surgeons are able to make up for this lack of haptic information by using their visual familiarity with the tissue. The pneumatic array developed by the CAISIT at UCLA aims to improve on *da Vinci* surgery by restoring some haptic information to the surgeon at the console.

Development of the pneumatic tactile display is detailed in [24] and [25]. To obtain force information, Cadere graspers were fitted with strain gages on the inner surface of the grasper tips. Cadere graspers are usually used to manipulate large tissues and objects, and provided ample space to



Figure 2-4. Tactile display fitted to *da Vinci* control. From [25].

mount reliable sensors. At the master console, the rotating control arms were fitted with tactile “displays” composed of an array of pneumatic balloons. The display was a polydimethylsiloxane (PDMS) balloon array manufactured from an aluminum mold with vertical columns to create the balloon space. The optimal array design was chosen after psychophysical experimentation [26].

The actuator balloons have a 3.0 mm diameter with 1.5 mm spacing, and arranged in a 3×2 pattern. The response time of the pneumatic display was 50 ms, and therefore had a frequency response up to 20 Hz, suitable for minimally invasive surgery. The pneumatic actuators were driven on a 0 to 15 psi output range. The design features a low mass and compact size, while delivering large forces and displacements. **Figure 2-4** shows the tactile display fitted to the *da Vinci* control.

Preliminary tests involved grasping a soft substrate (neoprene) strip covered in force sensing film with the modified tools [24]. Tests showed that using the haptic display generally reduced the force applied to the neoprene strip, demonstrating that improved haptic information can in fact reduce potential injury to “tissue.” Further work with this system is needed to clarify the benefit of improved haptic feedback on surgical performance. Continued development of this system towards higher fidelity haptic feedback would further bolster the compelling case to do surgeries minimally invasively whenever possible.

3 The Model-1 Hand-Held Force Magnifier

3.1 Model-1 Development

This chapter and the ones following it will describe the full development history of the HHFM from concept through two working prototypes. In reference to the HHFM, this text uses a coordinate system centered on the surgeon holding the tool. The “distal” end of the tool thus refers to the end of the tool furthest from the surgeon—the tool tip interacting with the patient’s tissue. “Proximal” refers to the end of the tool nearest to the hand. We shall also use the descriptor “axial” to describe actions, forces, or positions parallel to the long dimension of the tool. In context of forces, this will mean parallel to the device handle. In the context of torque, axial means rotational around the axis of the handle. “Lateral” refers to directions perpendicular to the axial direction.

This text also takes advantage of the inherent modularity of the HHFM, referring to force sensing assemblies and force actuation assemblies separate and distinct from one another. As long as there can be, in the future, a connection and interface between these two assemblies, they may be developed independently with no detriment to the performance of the overall HHFM system. Of course, refining both assemblies is clearly the best way to improve the performance of the HHFM as a whole.

3.1.1 Prototype Construction

Construction of the first proof of concept prototype, the Model-1, was completed in early November 2010 [11]. This first prototype features a commercially available force sensor (Honeywell FS01), mounted on a thin cylindrical handle made of brass. The Honeywell force sensor is a piezoresistive load cell with integrated electronics to condition and amplify its raw sensor signal to

produce a linear output signal. It can measure forces within a 0-6.8 N (680 grams) range with 0.165 N accuracy (2.5% of full scale). The short-term precision, however, is much greater—at approximately 0.005 N. Onboard conditioning circuitry provides for temperature compensation.

Eight rare earth permanent magnets (3/16" RadioShack 64-1895) are stacked at the proximal end of the brass body, and the entire assembly fits inside a coil of magnet wire, creating a solenoid actuator (250 feet of 30-gauge wire, 25 ohms, approximately 2360 turns) capable of pulling and pushing. The magnets are made of a Neodymium-Iron-Boron alloy, and have an average magnetizing force of 35,000 Oersted [27]. This assembly is mounted on a dual hinge or gimbal, which is fitted to a wrist brace. The gimbal assembly allows for lateral movement of the tool in both azimuth and altitude. Because the force sensor used in this prototype is a simple load cell, this first generation HHFM is only able to magnify “push” forces. **Figure 3-1** shows the completed Model-1 interacting with a spring phantom.

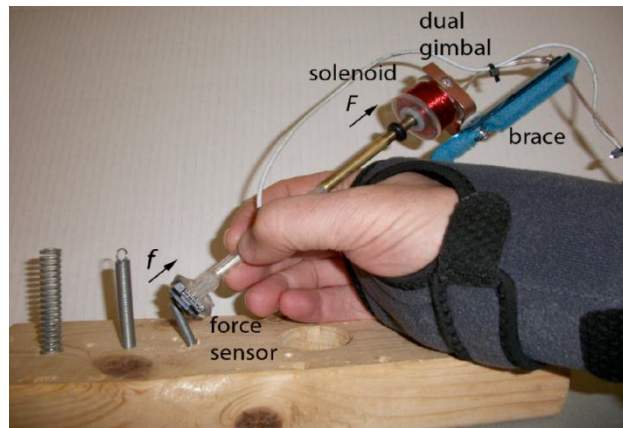


Figure 3-1. The Model-1 HHFM. [11]

3.1.2 Electronics and Control System

A schematic of the electronics controlling the Model-1 can be found in Appendix A. Control of the device is completely analog. A push-pull linear amplifier capable of supplying 32 V at 2 A is used to drive the solenoid. Amplification of the sensed force is accomplished with simple proportional gain, which is adjustable with a “gain” knob. Another control knob is used to calibrate the voltage across the coil to zero when the force sensor is unloaded, a process commonly known as “tare” in commercial scales used to weigh objects.

3.2 Model-1 Psychophysical Experiments

To investigate how users perceive and use the HHFM, preliminary psychophysical studies were conducted. Central to the experimental design is the Magnetically Levitated Haptic Device (MLHD), a 6 DoF haptic simulation tool developed by Ralph Hollis in the Microdynamic Systems Laboratory at Carnegie Mellon University and commercialized by Butterfly Haptics (Pittsburgh, PA) [28,29]. The MLHD has a bandwidth of 125 Hz at -3 dB, very fine position resolution (5-10 μm), and can exert stiffness

values from 0.005 N/mm to 50 N/mm, generating forces up to 140 N in the vertical direction and 55 N in the horizontal directions. Because force and motion are actuated by electromagnetic Lorentz forces, the device is free from static friction over its 25 mm diameter range of motion. These characteristics make the MLHD an excellent test bed for psychophysical experiments and haptic simulation.

In our experiments, six participants (four male), aged between 22 and 35, were tested under three conditions: control, HHFM-off, and HHFM-on. In the control condition, participants held an empty syringe body as a replacement for the HHFM. Participants were tested first in the control condition, and then in the HHFM on/off conditions. Participants were tested individually, with their eyes closed, and with active headphones to mask extraneous noise from the environment.

Our first experiment with the Model-1 sought to quantify the absolute lower limit in force perception with and without the HHFM. Participants were asked to touch the handle of the MLHD using the syringe or HHFM, at which point a series of forces were presented. The forces presented were always either clearly above (0.3-0.4 N) or below (0.0 N) perceptual threshold. Participants were then asked to press the “-“ or “+“ buttons on a keypad until the presented force had just disappeared or appeared. This force appearance/ disappearance procedure was repeated twice for each direction, and the force detection threshold was calculated as the mean of the four user-reported threshold values.

In our second experiment, we wanted to examine how users would perceive differential forces with and without the HHFM. The same six participants from the first experiment participated in the second. Force stimuli of 0.1, 0.2, 0.3, and 0.4 N were presented, and participants were asked to assign numbers to the stimulus based on its perceived intensity. The only restriction placed on the participants was that higher forces should be assigned higher numbers. Additional information on this magnitude

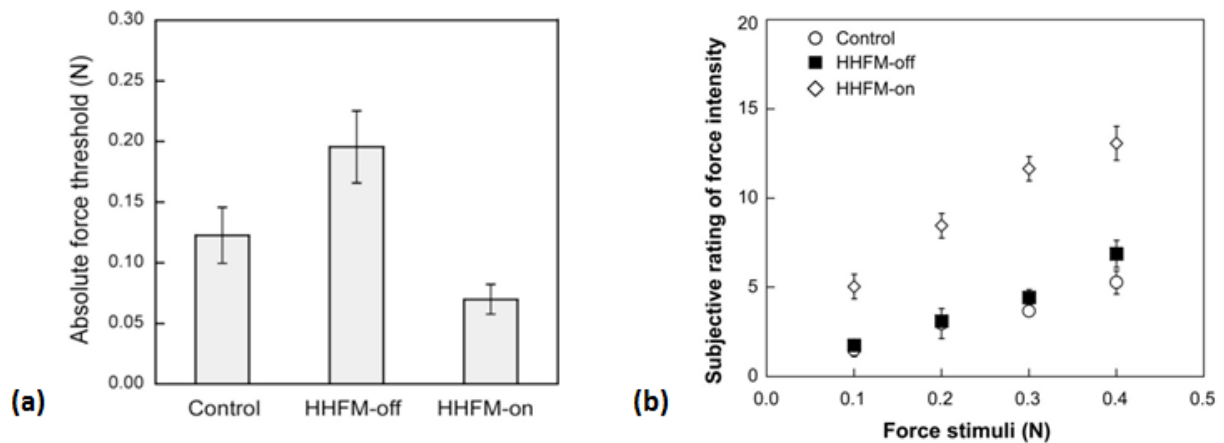


Figure 3-2. Psychophysical experiment results showing (a) improved force detection and (b) improved force discrimination. [11]

estimation procedure can be found in [30]. In the control condition, forces of 0.5, 1.0, and 1.5 N were presented to produce a similar response range for both control and HHFM trials, thus reducing the risk of range effects resulting from the HHFM magnification.

Results from both experiments are shown in **Figure 3-2a** and **3-2b**, respectively. We found that with the HHFM, users have a significantly lower absolute force perception threshold, proving our device can in fact augment a user's abilities beyond what is normally possible. Our second experiment was also successful, showing that the HHFM helped users differentiate between similar forces.

3.3 Model-1 Discussion

While the Model-1 worked well as a proof of concept, its design showed a number of weaknesses. The body of the device was prone to binding within the solenoid, which interfered with the amplification of force during use. Users with small hands in particular had a harder time using the Model-1 as a result of this binding, as well as the restrictive nature of the wrist brace. While using the HHFM for extended amounts of time during our psychophysical experiments, excess heat was generated by the solenoid to the point that the device needed to be turned off to cool.

4 The Model-2 Hand-Held Force Magnifier

4.1 Model-2 Development

Given the success of our initial psychophysical investigations, we began prototyping new designs for a HHFM able to magnify forces in both “push” and “pull” directions. Many configurations and intermediate designs were considered and constructed, and variation came mostly from different force sensing modalities. These intermediate designs included hydraulic, magnetic, and mechanical linkages, and various preload configurations.

4.1.1 Brace and Actuator Assembly

Because the brace to the Model-1 was restrictive and bulky, work was done to build a streamlined and better fitting brace and actuator assembly. **Figure 4-1** shows a design of the assembly using SolidWorks, which was subsequently constructed of aluminum stock and acrylic tubing. The two-piece brace is a simple hinge, and is secured to the hand by Velcro straps (not shown). Foam padding was added to the back of the brace to improve fit and comfort. A rotary bearing was press-fit into the top of the brace, to allow for movement of the actuator assembly in azimuth. A small post was press-fit into the rotary bearing and extends vertically to connect to a new gimbal. The gimbal features a crossbar, which allows for

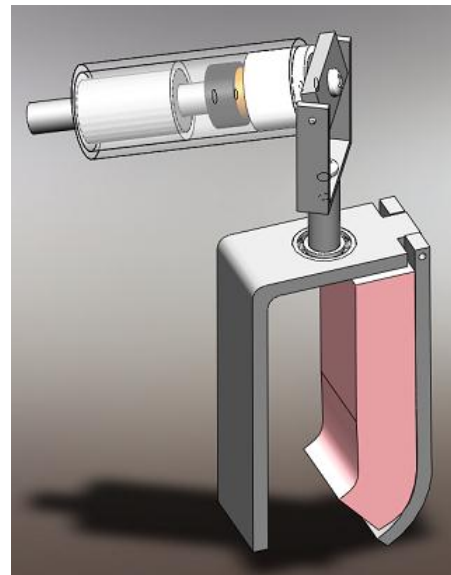


Figure 4-1. Model-2 brace and actuator assembly (SolidWorks)

movement in altitude and serves as the attachment point for the actuator. Compared to the Model-1 brace, this new assembly is much easier to put on and take off, and makes the HHFM easier to adjust for those with small hands. Because of the better fit, the connection to the hand is more solid, forming a better base from which forces can be actuated.

The homemade solenoid in the Model-1 was replaced in the Model-2 with a commercially available voice coil (Moticont LVCM-19-022-02) capable of generating up to 2.5 N of force over its 12.7 mm stroke length. Voice coils differ from solenoids only in the component that moves. In a voice coil, a coil of current-carrying wire moves inside of a stationary magnetic housing, whereas solenoids feature a moving metallic or magnetic bar in the presence of a stationary coil. The principle of movement based on electromagnetic mechanisms is equivalent in either configuration, of course. Voice coil actuators tend to be smaller and faster, as the moving coil of wire can be light for relatively high strength stationary magnets. The Moticont actuator measures only 19.1 mm in diameter with a 22.2 mm long housing.

The housing of the voice coil is secured to the brace crossbar by a machine screw. An applied voltage across the motor terminals causes movement of the coil in one direction, while reversing the voltage moves the coil in the opposite direction. An aluminum post is secured to the coil with a machine screw, and supported by a concentric linear bearing to allow the coil to move freely in the magnetic housing. These two parts—the magnetic housing and the linear bearing—were in turn press-fit and glued into concentric acrylic tubes, holding them in an appropriate configuration to permit force generation. At the distal end of the moving post, a through hole was machined to interface with various sensor assembly designs.

4.1.2 Hydraulic Pressure Sensor Prototype

The first sensors in our Model-2 prototype were focused around small, fluid filled pressure sensors (Motorola MPX2011DT1). These sensors were chosen on account of their small size (6.60 mm × 6.07 mm × 3.81 mm), high sensitivity (full scale pressure limit of 75 kPa), and low cost (less than \$1). Knowing the diameter of the diaphragm (2.41 mm), we can estimate full scale force limit to be 435 mN, which, given their dynamic range of at least 100, is sufficient to measure the forces characteristic of ophthalmic surgery. A silicon piezoresistive strain gage arranged as a Wheatstone bridge is the heart of the Motorola sensor, and this interfaces with the outside world through a dielectric silicone gel, which transmits pressure uniformly across a diaphragm. A small amount of gel between the diaphragm and the piezoresistive strain gage serves as a force transmitter. As such, these sensors can measure applied

forces in both directions, since the strain gage will be displaced in opposite directions by push and pull on the diaphragm and gel. Because the sensing element is configured as a Wheatstone bridge, the output voltage can be positive or negative. The pressure sensor includes some limited integrated temperature compensation and calibration, and uses materials previously approved in medical applications.

Our first sensor assembly using the Motorola pressure sensor was a hydraulic assembly. **Figure 4-2** shows this hydraulic assembly. The assembly consisted of the pressure sensor glued to the needle end of a syringe (with the needle removed). The

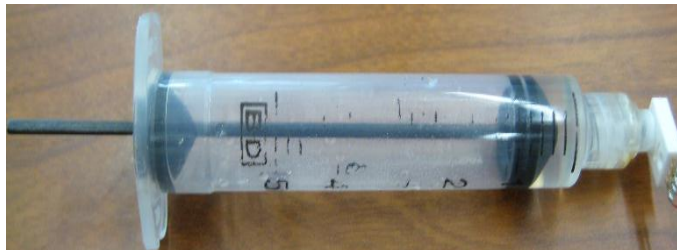


Figure 4-2. Hydraulic Pressure Sensor Prototype.

The sensor end was filled with 20 mL of water, and the rubber plunger inserted into the syringe and advanced until a moderate pressure was applied to the sensor. Because water is extremely incompressible, the volume of water will be able to transmit the tissue forces without significant displacement. Of course, this is only true as long as the diaphragm at the interface of the air and water (at right in **Figure 4-2**) deforms and returns to its initial position when unloaded. The plunger was modified to include a long carbon fiber rod as the “tool tip,” pulling or pushing on the plunger as the user interacted with the environment. A second plunger (at left in **Figure 4-2**) was used to center the carbon fiber rod at the tool’s distal end, without adding unduly to the total spring constant of the system. Rubber plungers were chosen because static frictional forces between the plunger and the syringe body would resist displacement of the whole plunger when loaded, thus maintaining the sensor preload. Carbon fiber was chosen because of its high stiffness, ensuring that little energy is lost due to strain in the tool tip when interacting with tissue.

Furthermore, studying the signal from the pressure sensor, we very quickly understood a practical difficulty of a liquid pressure system. Over long time scales, the assembly was subject to heavy dependence on external temperature, because water expands and contracts thermally in its chamber, biasing the pressure sensor signal. Thermal expansion of the syringe body also affects the preload as the volume of the chamber changes with temperature. The piston, being the rubber plunger cover fitted with a long carbon fiber rod, was too stiff to produce measurable pressure changes for small forces. Yet, even with this first sensor assembly, we were impressed with the short-term stability of the pressure sensor signal in steady-state conditions.

A major appeal of the hydraulic approach was the possibility of having the sensor in the proximal portion of the tool while sensing forces distally by means of a hollow tube, such as are common in medical needles. We were intrigued with the prospect of amplifying force through use of a “master” piston at the tip of a needle, with a smaller surface area than that of the sensor. This concept proved illusory, since such gain in force cancels with the common currency of pressure, and we decided to move away from hydraulic linkages toward direct mechanical linkages.

4.1.3 Guidewire Pressure Sensor Prototype

The next prototype with the Motorola pressure sensor (see **Figure 4-3**) featured a length of catheter guidewire (from the stiff end of a guidewire from a peripherally inserted central catheter kit) as the connection to the pressure sensor. One end of the guidewire was dipped and rolled in 80-20 quick setting epoxy (RadioShack #6400099), and allowed to dry as a roughly spherical bead. This bead was then fastened to the pressure sensor diaphragm using silicone, so that the guidewire extended directly from the sensor diaphragm. **Figure 4-3** shows this attachment scheme. To allow a user to hold the sensor assembly, a handle was fashioned by gluing a needle guard to the sensor housing, allowing a user to interact with the world through the free guidewire tip.

We used string as a way to center the guidewire at the distal end of the handle, and to restrict motion to the axial direction (see **Figure 4-4a**). This initial realization suffered from high sensitivity to lateral forces, but the resin bead turned out to be a sensitive relatively stable way to connect forces at the tool tip to the pressure sensor.

A more advanced prototype of the guidewire sensor

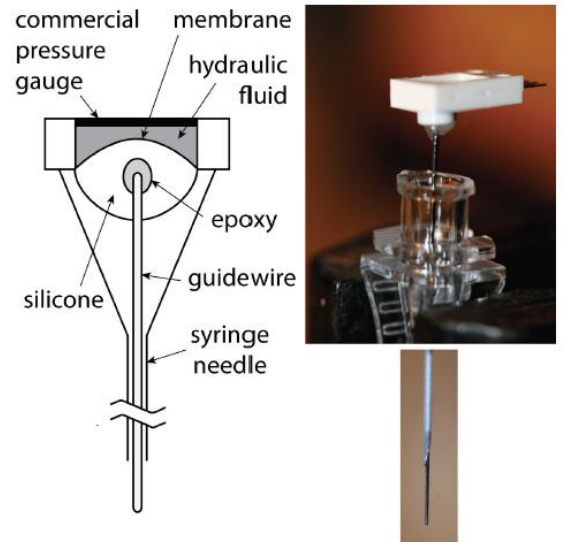


Figure 4-3. Guidewire pressure sensor prototype.



Figure 4-4. (a) string guided pressure sensor and (b) needle hub pressure sensor

assembly shown in **Figure 4-4b** used a syringe needle as the method of restricting lateral motion in the guidewire. The guidewire was inserted into a dull needle, with its free end still able to move in the axial direction as the tool interacts with the world. A secondary housing was fit around the needle hub, and a Delrin bushing was machined to hold the needle tip concentric with this outer housing to protect against shear stresses that would have confounding axial components. Delrin is a polymer with good stiffness and low frictional coefficients, making it a good material for linear bearings. Acrylic pieces were machined to fit around the pressure sensor at the end of the needle hub, forming a chamber large enough to house the sensor and some simple amplifiers, and to connect to the actuator and brace assembly.

A rough calibration experiment was first performed to better understand the behavior of this sensor assembly alone. The sensor assembly was oriented in the vertical direction, with the free end of the guidewire closest to the ground. A lightweight plastic tube was attached to the guidewire and the sensor voltage was allowed to stabilize. Pieces of wire of uniform length were cut and loaded into the tube, with an average mass of 0.47 g, and loading curves were obtained as shown in **Figure 4-5**. The assembly was loaded twice, using the same sequence of load masses. The force sensor was given 5 minutes to re-stabilize before the second loading sequence.

As can be seen, the load response of the sensor was quite linear. However, the loading curves show a measurable drift in the sensor output, with the sensor unable to return to its initial voltage after being unloaded. This could manifest for a number of reasons. Friction between the guidewire and

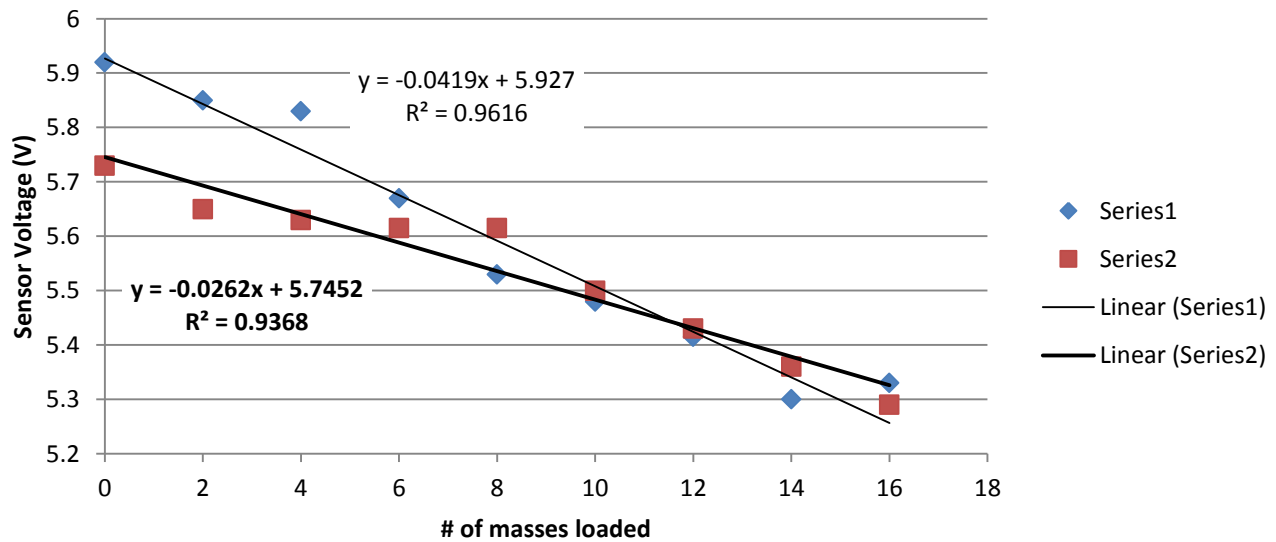


Figure 4-5. Hysteresis between loading cycles for needle hub pressure sensor prototype.

needle as it moves through the needle could confound the spring response of the diaphragm and resin connection. Our string prototype saw a better spring response because it was connected to the outside housing at only one point, in such a way as to present minimal axial forces. Further, non-linearity and hysteresis was probably due to the viscoelastic behavior of silicone connecting the epoxy bead to sensor diaphragm.

In the end, the Motorola fluid-filled pressure sensor was abandoned in favor of a mechanically actuated force sensor, but important lessons were learned from these initial sensor assemblies. Hydraulic force sensing systems, though they have the advantage of being predictable and governed by well-known laws, are hard to calibrate and maintain as stable sensors. Mechanical connections are more reliable and easier to assemble, but size constraints restrict our designs so that long appendages are necessary to interface with the sensor. As mentioned previously, these long tools generate unintentional moments and can magnify tremor through a lever arm effect. The guidewire is affected in exactly the same way—small lateral forces at the distal end generate large moments at the proximal sensing end. With our one-dimensional sensor, the axial component of these moment forces confounds our measurement of tissue forces at the tip. This results in errors in the estimated tissue force, which in turn distorts the force actuated to the hand.

4.1.4 Magnetically Stabilized Prototype

We replaced the Motorola pressure sensor with a small force sensor (Honeywell FSS1500N). Compared to the Motorola sensor, the Honeywell sensor is equally small (9.14 mm × 5.59 mm × 3.25 mm) and again uses silicon piezoresistors arranged in a Wheatstone bridge as the sensing element. Because the FSS1500N sensor is a one-directional load cell like the bigger FS01 sensor used in the Model-1, a method of preloading the sensor was necessary to be able to differentiate between push and pull actions. A stainless steel ball enclosed by the tough plastic housing transmits force directly from the tool tip to the sensing element. The FSS1500N sensors have a nominal operating force range of 1500 grams, but are designed to withstand up to 4500 grams force. Importantly, sensors have an average sensitivity of 0.12 mV/gram on a 5 V supply voltage. Unlike the FS01, the FSS1500N does not include onboard signal conditioning and temperature compensation.

In our previous prototypes using the Motorola pressure sensor, problems arose because we could not accurately and reliably reproduce our preload or zero-point, introducing error in our sensor signal. In this prototype, we decided to investigate the use of permanent magnets as a way to generate our sensor preload in a reproducible way.

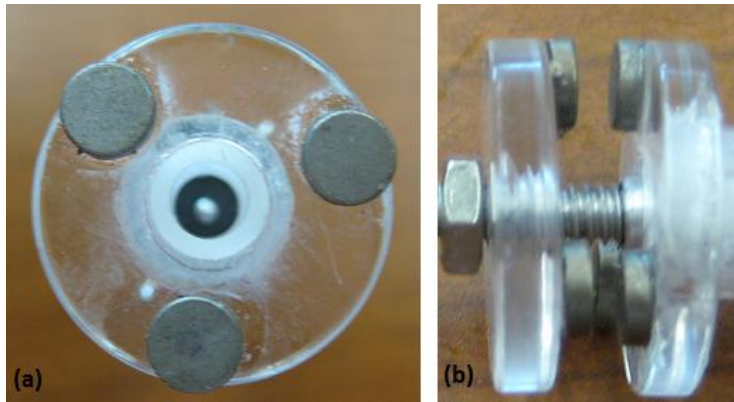


Figure 4-6. (a) Triangular arrangement of rare earth magnets (b) Magnetically stabilized preload assembly

First, a handle was fashioned to hold the FSS1500N at the end of an acrylic tube which would interface with the brace and actuator assembly. Notches were cut into the proximal end of the handle and a sensor was press fit in place. Three rare earth permanent magnets (3/16" Radio Shack 64-1895) were glued to two 0.75 inch diameter acrylic discs as shown in **Figure 4-6a**. The polarity of the magnets was arranged so that the two discs could then be attracted to each other as shown in **Figure 4-6b**. The distal disc was tapped in the center to fit a 6-32 aluminum threaded rod, while a center hole in the proximal disc was drilled to match the acrylic handle interfacing with the actuator. A Delrin foot was machined to screw onto the end of a 6-32 threaded rod, contacting the FSS1500N with a smooth, flat surface. A thin aluminum sheath was machined to fit over the threaded rod, and Delrin bushings were machined to restrict lateral motion but not axial motion. The bushings were glued into the acrylic housing. **Figure 4-7a** shows the threaded rod assembly, and **Figure 4-7b** shows the entire force sensing assembly as attached to the HHFM handle.

The sensor preload was controlled by adjusting the distance between the magnets on the distal disc and the Delrin foot where the threaded rod contacts the stainless steel ball. Orientation around the tool axis of the triangular arrangement was important, as the magnets were implicitly paired when they were glued to the discs as described earlier. Mismatches between



Figure 4-7. (a) Threaded rod assembly with Delrin bushings (b) Magnetically stabilized sensor prototype connected to HHFM

magnetic pairs could result in the plunger being loaded slightly laterally. A spacing of approximately 0.50 inch (12.7 mm) is kept between the opposing sets of magnets.

The last remaining piece of the HHFM system was an electronic system to produce amplified forces in response to measured force at the tool tip. While the analog circuitry and digital control units are described in greater detail in *Section 4.1.7*, the general workflow regarding operation of the HHFM system is described here. First, the signal from the force sensor assembly is measured and digitized. The signal is then compared to a stored preload value, and the difference between the two numbers taken to obtain the magnitude and direction of the measured force. This measured force is then amplified by multiplying by a gain value and outputted as a voltage to drive the voice coil. This process operates with a bandwidth of approximately 1 kHz, producing amplified forces that mirror those measured in the tissue without noticeable delay.

In this magnetically stabilized sensor prototype, a National Instruments (NI) USB 6009 DAQ (data acquisition unit) was chosen as the hardware hub. The DAQ was programmed in LabVIEW, a graphical programming language that uses “virtual instruments” (VIs) to control a connected DAQ. An advantage to LabVIEW is that it can be used to log and store data for future analysis, and certain constants, like the gain or the offset value, can be changed as needed in a graphical user interface (GUI) running the VI.

As a full system, the magnetically stabilized prototype performed well when in direct contact with an object, although the haptic illusion was not as pronounced as in the Model-1 prototype. Adjusting the gain in general improves the haptic effect, but also increases noise in our output signal. Noise in the actuator signal is sensed as vibrations. While using the HHFM, hysteresis effects were also seen, and the offset value would need to be recalibrated often to avoid generating a bias force in the voice coil. The hysteresis was most likely due to effects arising from contact between the Delrin bushings and the aluminum sheath. While thermal expansion of the metal contacts (aluminum rod and stainless steel ball) is negligible at the room temperature, expansion of acrylic plastic could be significant. Minute changes in the preload distance, which can originate from variation in the thickness of the proximal acrylic discs, will drastically affect the preload force because static magnetic forces scale approximately with the square of the distance between magnets [31].

When left idle, we found that the HHFM was prone to produce audible oscillations from the voice coil. Our initial suspicion regarding the source of this feedback was high frequency electromagnetic interference being picked up by our assembly or by sensor wires. Because of its small size, the FSS1500N does not contain additional circuitry to shield the sensor from high frequency noise. Adding low pass filters in the analog circuitry did not totally resolve the problem, however. To

investigate this issue further, we repurposed the control VIs to also log sensor data while the device was in use. **Figure 4-8** shows a time plot of the raw sensor input voltages (red) and the amplified output voltages (green) driving the voice coil as a stationary HHFM was pushed and pulled. Spikes in the raw sensor signal indicate a “push” motion, while a “pull” motion is evidenced by a dip in the raw sensor voltage.

While the sensor voltage itself isn’t particularly noisy, our amplification is all encompassing, and produces the chaotic output signal driving the voice coil as shown in green. The hardware interface was designed to use 2.5 V as the “zero point” for the voice coil, the voltage at which the voice coil does not generate any force. Voltages in the range 0 – 2.5V drive the actuator in one direction, while voltages in the range 2.5 – 5V drive the actuator in the other direction. Amplification of noise about the 2.5V midpoint would explain why the voice coil oscillates audibly when the HHFM is idle. Indeed, when loaded, the generated voltages saturate and steady forces are generated by the voice coil in response, eliminating all oscillations. The problem of noise amplification is compounded because the sensor and actuator assembly are now mechanically connected, leading to a positive feedback cascade. The stability of the system thus depends on whether forces are being applied to the sensor.

While the magnetically stabilized prototype had some considerable shortcomings, it is important to highlight areas of improved performance compared to the first prototypes. The magnetic preload was wonderfully reproducible, as evidenced by the raw sensor signal data. Sensitivity to lateral forces was still measurable, but improved considerably with the addition of the Delrin bushings within the acrylic housing. The lessening of hysteresis effects when loading the sensor laterally further supports the claim that frictional forces in the axial direction drive the overall hysteresis seen in the HHFM. The workflow process controlling the HHFM also worked well, and its general structure was used in future iterations. Overall, the full assembly was easy to hold and use, and worked well enough to be a proof-of-concept for bidirectional force sensing and actuation.

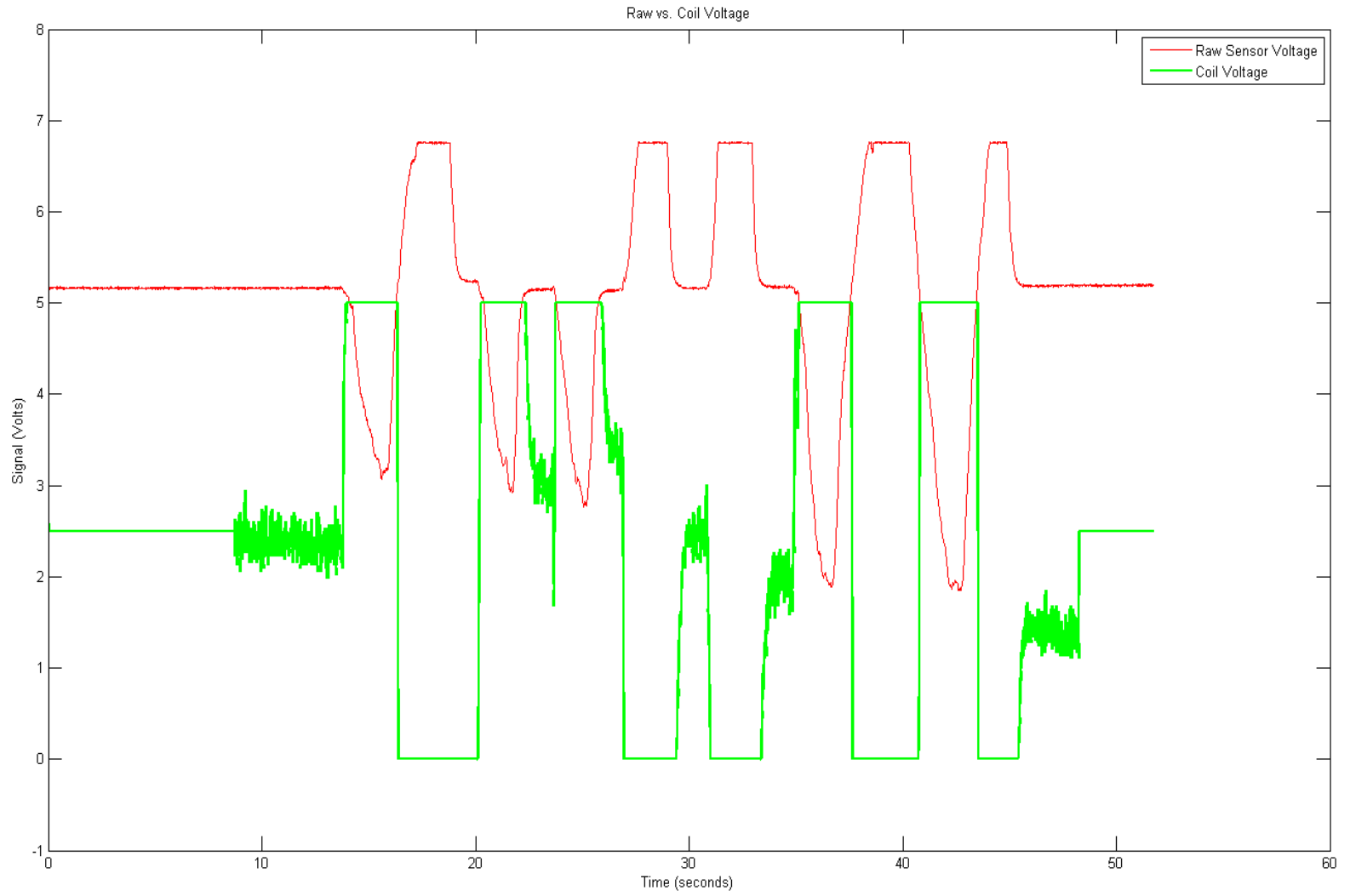


Figure 4-8. Data from VI logging with raw sensor signal (red) and sensor output signal (green).

4.1.5 Leaf Spring Preload Prototype



Figure 4-9. Leaf spring design in triangular arrangement.

Because we now better understood the consequences of directly amplifying noise in a sensor signal, we began to design new force sensor assemblies focused on achieving the minimum amount of noise. To this end, we again adopted the Honeywell FS01 force sensor as the basis for our device. We also wanted to better minimize the effect of lateral forces confounding our axial force measurements. This was attempted with a “leaf spring” design as shown in **Figure 4-9**. In this design, strips of shim stock metal are used as custom springs, and arranged in a triangular configuration to equally resist moments due to lateral forces. The leaf springs would also apply a constant preload to the sensor, as determined by the Delrin spacers. Because of the small displacement exhibited by the sensors, the preload should remain constant.

Two 3/4 inch (19.05 mm) diameter acrylic discs were used as the base for the force sensor assembly, stacked on top of each other. The FS01 sensor was glued to the distal disc face, while the proximal disc face was connected solidly to the device handle. The leaf springs were then fashioned from a sheet of 12 mil (0.012 inches, 0.305 mm) thick stainless steel shim stock. Pieces of shim stock were cut into 1/4 inch wide (6.35 mm) strips of varied lengths. At one end of each strip, a 1/16 inch (1.58 mm) diameter hole was drilled in the center of the strip, 1/8 inch (3.175 mm) from the edge, to allow the carbon fiber rod to pass. Four Delrin spacers were machined to be 1/8 inch tall and 1/4 inch in diameter. 1/16 inch holes were drilled through the Delrin spacers to accommodate the carbon fiber rod that was to interface with the FS01 sensor. Along the length of the carbon fiber rod, spacer and spring were stacked alternately on top of each other. Two right angle bends were made in each leaf spring—one to clear the lateral distance from the carbon fiber rod and to bring the spring parallel to the axis of the tool, and another to bring the free end of the spring between the two acrylic discs.

With this force sensor assembly driving the HHFM, we saw many of the same problems as in the magnetically stabilized force sensor, and for very similar reasons. The HHFM was found to drift, which could be attributed to thermal expansion of the Delrin spacers changing the spring preload. Lateral effects were still present because shim stock would tend to rotate at the proximal acrylic base, even though the free ends were solidly connected to the device handle. A simpler mechanical design and an improved hardware interface were adopted to address these problems.

4.1.6 Shim Stock Preload Prototype

In our final design, bidirectional force sensing was accomplished by constructing a cage around the force sensor to apply a constant preload. Each part of the assembly that could affect preload was constructed of metal instead of plastic, to reduce thermal effects. The FS01 sensor was glued to an aluminum base, with tapped holes in the corner to allow aluminum spacers to be rigidly attached. A square piece of the 12 mil stainless steel shim stock was used serve as the spring. A hole was drilled into the middle of the stainless steel shim shock and a threaded rod was passed through, interfacing directly with the sensor. Wide washers and nuts threaded onto the rod were used to resist generating rotation at the pivot point. The sensor contact point was rounded so that the radius of curvature at the contact point was approximately the same as the distance between the sensor plunger and the pivot point. In this way, rotation at the pivot point would not result in axial motion of the sensor plunger. **Figure 4-10** shows this prototype.

As will be seen in more detail in the next section, the NI USB DAQ controller was replaced because of its unreliable sampling interval. A microprocessor (Analog Devices ADUC7026) was chosen instead, in particular, a board-level development kit using the microprocessor. The microprocessor uses the “C” programming language and contains a number of analog-to-digital (A/D) and digital-to-analog (D/A) converters. Programs on the microprocessor run with only the user-defined interrupts, not subject to the operating system (OS) and background routines that give the NI USB DAQ its unreliable frame rate.

The new force sensing assembly returns quickly to its preload when the device is in use, although the sensor assembly needs time to stabilize before it can be used reliably when initially turned on. This warm up period is approximately 30 minutes. Gain, tare, and any other parameter of the



Figure 4-10. Shim stock preload prototype.

program is accessible through panel mounted potentiometers and switches, although care must be taken not to introduce noise into the signal by continuing to resample potentiometers. With the new hardware, we are able to sample at a rate of 10 kHz, allowing the HHFM to react very quickly to changing forces. However, to avoid sampling artifacts, we filter the analog inputs at approximately 1 kHz.

4.1.7 Electronics and Control Systems

Electronics schematics for the final iteration of the Model-2 can be found in Appendix B, along with the LabVIEW VI and Analog Devices controller code. While control over the HHFM is still open-loop, digital computer systems were integrated to more precisely regulate HHFM behavior. Currently, three power supplies provide power separately to each of the following components: the analog circuitry, the CPU, and the actuator. Careful attention has been paid to voltage regulation and grounding, so that currents in one part of the system do not affect voltages in another. The circuitry and microprocessor



Figure 4-11. Front panel to Model-2 electronics enclosure

board were housed in a small aluminum box, making it secure and easily transportable. **Figure 4-11** shows the front panel of the second generation electronics enclosure for the HHFM.

Our magnetically stabilized and leaf spring prototypes were controlled using a NI USB 6009 DAQ, which features 14-bit A/D input resolution over 20 V, and a maximum analog input sampling rate of 48 kS/s.

The USB 6009 also features 12-bit D/A output resolution over 5 V. While LabVIEW is a relatively intuitive and easy to understand programming language, the learning curve is steep and its graphical nature makes debugging and performance verification difficult. Because LabVIEW runs within a computer environment, it is also subject to OS level interrupts which interfere with DAQ performance. For example, **Figure 4-12** shows oscilloscope readings of voice coil voltage in the magnetically stabilized prototype when connected to a computer with either a Macintosh OS (OSX) or a Windows OS (Windows 7). We can clearly see a reduction in overall noise when the HHFM was connected to a Macintosh

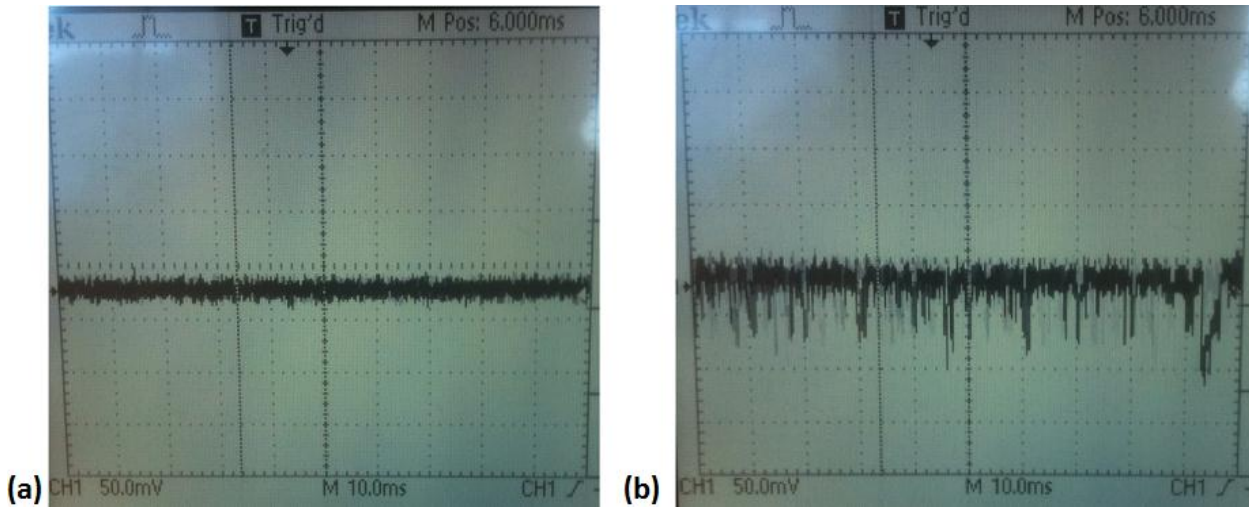


Figure 4-12. Oscilloscope with NI DAQ on (a) OSX and (b) Windows 7

operating system. The period between sampling events was also inconsistent between operating systems, as shown in data logs in **Figure 4-13**. This undesirable feature in the controller likely accounted for some of the poor behavior seen in the magnetically stabilized and leaf spring prototypes.

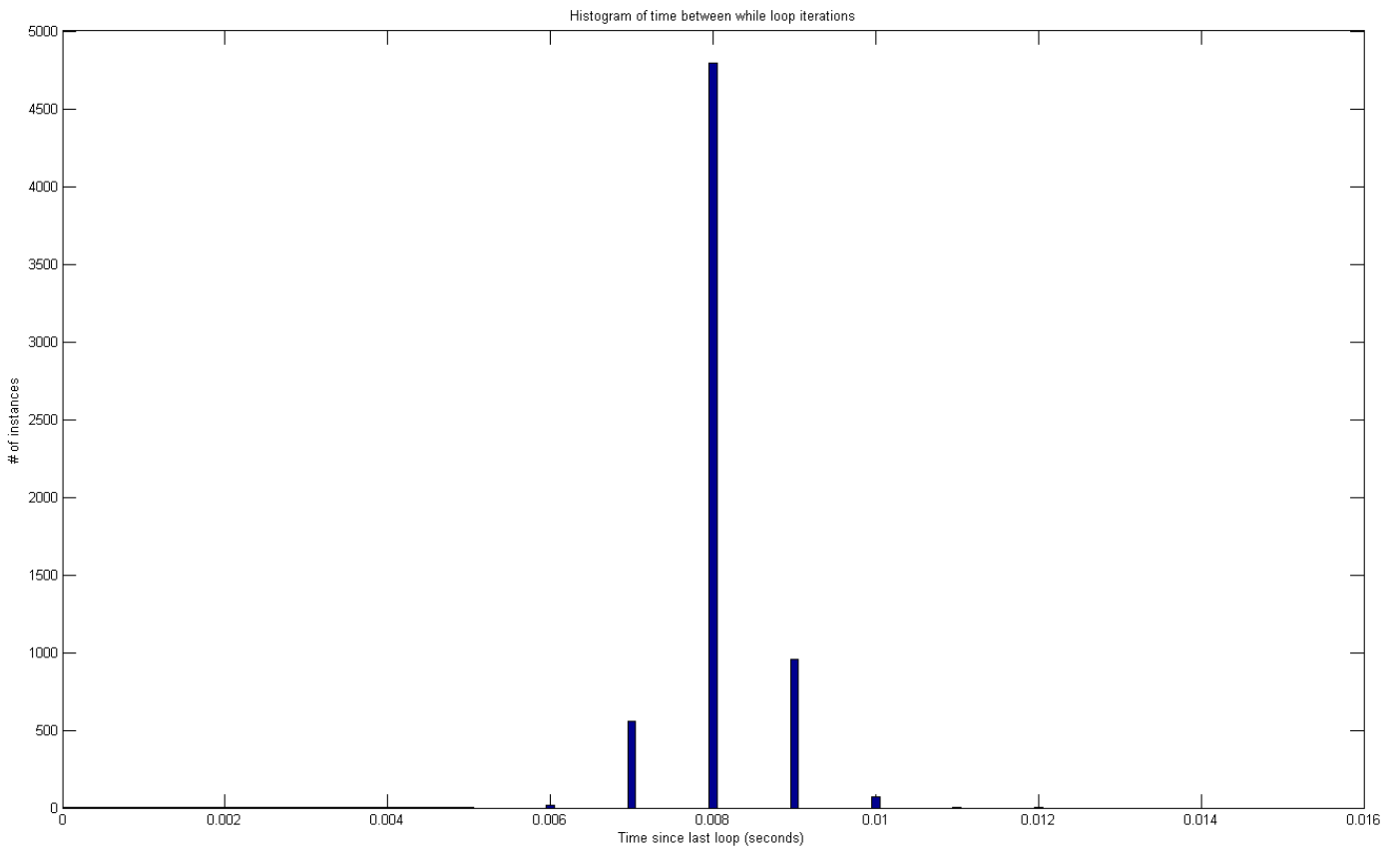
To replace the NI DAQ, an ADUC0726 microprocessor from Analog Devices was adopted to control HHFM behavior beginning with the shim stock prototype. The 41.48 MHz processor is integrated to a development board with 12 A/D channels, 4 D/A channels, and 40 digital input/output (I/O) ports. Each analog input and output is capable of sampling at rates up to 1 MS/s at 12-bit resolution. The CPU is flash programmable via a USB connection, but operation does not require tethering to a computer, as was the case with the NI USB 6009 DAQ. The control programs are written in C and control the CPU directly without other programs or an OS running in the background.

With these new capabilities, some relatively advanced behavior was extended to the HHFM. We were able to reliably increase our sampling and output rate to 10 kHz without significant jitter using CPU interrupts at that frequency, and a guaranteed within loop processing time of less than 100 microseconds. The problem of measuring and maintaining an accurate preload voltage was solved by sampling the sensor voltage over a full second. However, instead of sampling a full 10,000 points, only 200 samples were taken, at randomly generated intervals during the second period to avoid sampling aliasing effects. A button was also added to “mute” the response of the voice coil, to isolate the performance of the sensor from the actuator, while keeping the two assemblies mechanically connected. For example, when setting the preload voltage, the voice coil is muted to avoid mechanical

feedback effects in the sensor signal. A final button was also added to reset the CPU, which eliminated the need to open the enclosure if a hardware reset was necessary.

While the new CPU allowed a number of improvements, the inability to easily log data restricted our capabilities to fully understand and characterize our design. To further refine the control programming, we wrote a VI program to log voltages coming into and out of our hardware interface, using the NI USB 6009 DAQ. We logged data while running two versions of the HHFM code, one where the gain multiplier was obtained from a potentiometer knob at every loop, and one which saved the gain value only once, when calibrating the instrument to its preload. The data logs are shown in **Figure 4-14**. As we can see, being judicious as to when potentiometer settings are interrogated and used can provide much improved results.

(a)



(b)

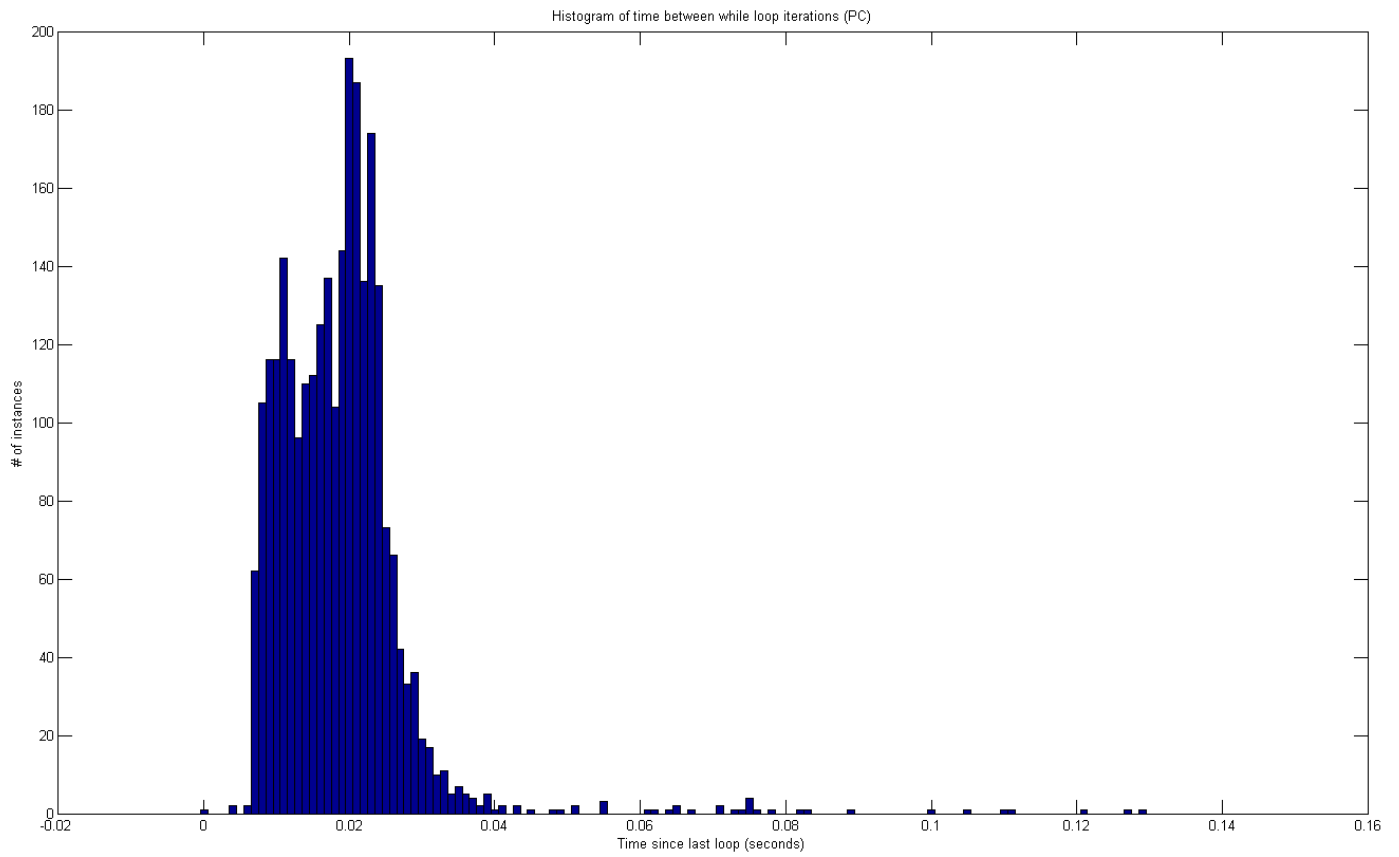


Figure 4-13. Histograms of sampling times with HHFM connected to (a) OSX and (b) Win7

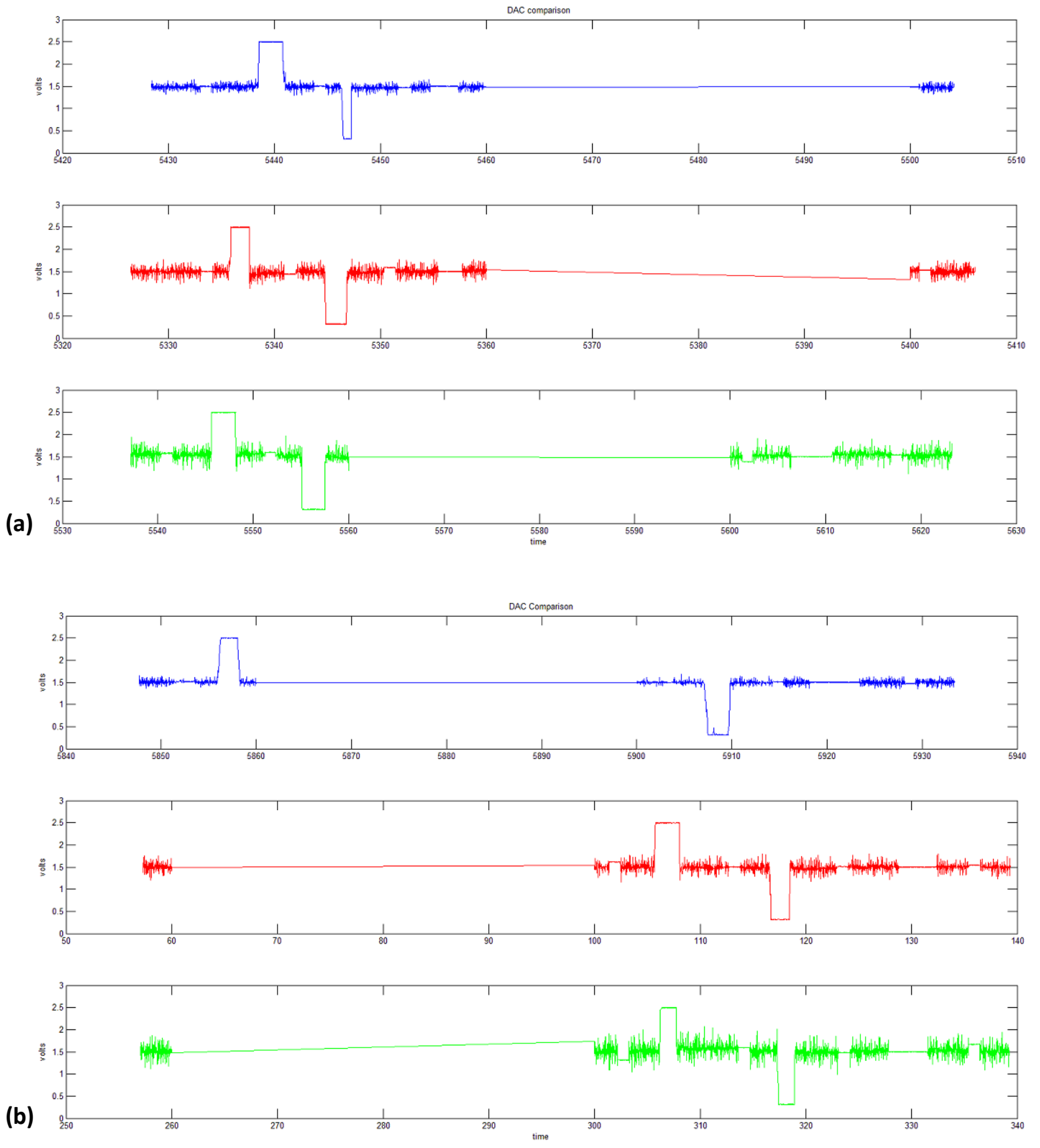


Figure 4-14. Coil signals with (a) knob computed gain and (b) hardcoded gain. Blue shows gain of 15, red is gain of 30, and green is gain of 45.

4.2 Model-2 Psychophysical Experiments

Psychophysical studies using the Model-2 are currently underway. In this new series of studies, we are examining operator behavior as the HHFM is used to pierce a simulated membrane. Our continued collaboration with CMU Psychology Professor Klatzky, as well as with CMU Robotics Institute Professor Ralph Hollis, has included graduate student Vikas Shivaprabhu to develop software for the MLHD as the mechanism to conduct our studies.

To interface the HHFM with the MLHD, a connector was machined out of aluminum stock to connect the HHFM directly with the MLHD flotor. The bottom piece was secured to the flotor using brass screws, and a rotating top half connects to the HHFM with a threaded hole. The wide operating angle of the HHFM connection point allows for any attack angle that is comfortable for the participant. **Figure 4-15** shows the MLHD with connector attached to a “dummy” HHFM for baseline experiments.



Figure 4-15. MLHD interface with dummy handle.

As will be further elucidated from psychophysical testing, “skid” after puncturing a membrane is a real danger to using the HHFM in delicate surgery. In this context, skid refers to unintentional movement observed after being released from tissue forces, i.e. after piercing a membrane. Carefully characterizing this behavior will be essential in finding technological ways of minimizing it. Preliminary, unpublished data reveals that user behavior is largely based on *physical* laws immediately following

membrane puncture. After a characteristic time, data seems to show that behavioral similarity among users breaks down, and physiological variability comes into play. In other words, there is a delay in reaction after having punctured a membrane. Braking mechanisms or other methods to eliminating unintended behaviors will need to be incorporated into successive generations of the HHFM.

4.3 Model-2 Discussion

Throughout development of the Model-2, modularity in our design allowed for efficient experimentation. Our brace and actuator assembly remained largely the same throughout the development process, while we exchanged force-sensing designs. In the same way, after our initial workflow was found to work using the NI USB DAQ, it was left essentially unchanged as we moved on to the Analog Devices processor.

Arguably, sensing forces in a constrained space was the most difficult aspect of designing a working Model-2 HHFM. By easing the size restriction, we were able to focus on designs that worked well to sense force in the context of surgical instruments. From this platform, we can refine our future designs to better fit the constraints of ophthalmic surgery. In using the HHFM, it was seen that the preload sensed would change with orientation of the device due to gravity. As a result, our voice coil would be biased in one direction, giving the peculiar illusion that the tool was getting heavier as we turned it towards the ground. This problem can be solved by integrating an accelerometer to measure and compensate for changes in orientation.

Solving some circuitry problems, like noise and voltage drops in power buses, greatly improved performance. However, we could probably improve it further, as well as reduce the number of power supplies, simplifying design for a sterile operating theatre in future work.

5 Future Work and Conclusion

5.1 Model-3 and Beyond

In future prototypes, work will be done to reduce the size of the sensor assembly to better fit the constraints of ophthalmic surgery. Great potential exists to reduce the size of the force sensor, now that a successful design has been proven in the shim stock cage prototype. Of course, noise is a primary constraint with smaller sensors, so careful decisions must be made regarding the components for the Model-3. Extremely small (2.5 mm x 3.3 mm x 1.3 mm) surface mount pressure sensors (Merit 3000 series) are proposed in this prototype of the Model-3 shown in **Figure 5-1**.

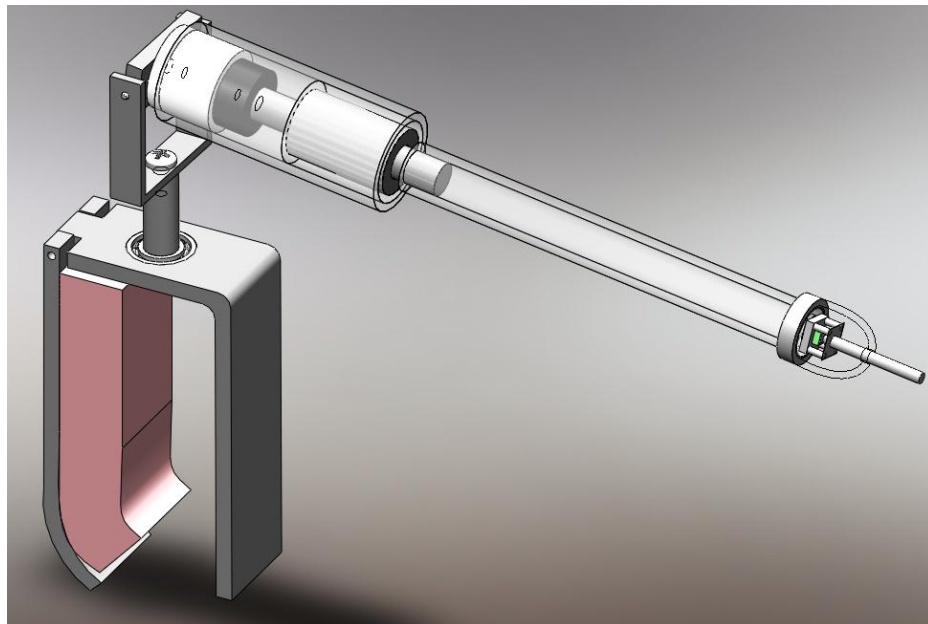


Figure 5-1. SolidWorks model of Model-3 HHFM with Merit sensors

While the Model-2 brace and actuator assembly worked extremely well through all of the various prototypes, we found that voice coils introduce too much variability in force generation because the force produced for a given current depends on the position of the coil in the magnet housing. It would be beneficial to find an actuator that can generate forces independently of position. As one possibility for the Model-3, we have identified the Squiggle motor, a tiny linear motor that actuates movement through piezoelectric principles. The SQL-3.4 motor is able to generate stall forces as high as 2 N, over its 7 or 20 mm length [32]. The motor in its housing measures 6.83 mm in diameter and 11.02 mm in length. The issue of speed and latency needs further investigation.

Refinement of our control programming to include advanced, automatic behavior would be preferred. For example, an automatic tare function, with orientation compensation, would be extremely useful. Particular compensations for unwanted actions of the HHFM, “skid” behavior following membrane puncture, for example, could be addressed by specific algorithms. Preliminary data suggest that we can precisely characterize reaction delay and its variability among users. With this information, we could fashion braking systems to handle the large force differentials associated with membrane puncture.

5.2 A Commercial Future for the HHFM

As part of my Masters program, I have participated in a special course called “Bench to Bedside,” in which we have prepared an application for Coulter Foundation funding towards commercial development of the HHFM. We have identified ophthalmology as an initial application for the technology. There are currently no commercially available devices that attempt to solve the haptic problem in ophthalmic surgery. The market is saturated with traditional microsurgical tools, only distinguishable from tools used in general surgery by the fact that they are smaller, more delicate, and better suited to the workspace and tissues of the eye. The market leaders in this application are large corporate entities including Alcon, Bausch & Lomb, Abbott Medical Optics and Johnson & Johnson. While we have seen that surgical tools that improve the sense of touch in microsurgery are a popular academic research topic, none of these projects have advanced to the stage of commercialization.

5.2.1 The Unmet Clinical Need and Market Size

Collaborating with Dr. Joel Schuman, Chair of Ophthalmology at the University of Pittsburgh Medical School, we propose development of the HHFM for use in anterior segment surgery, surgeries of the cornea, lens, and surrounding tissues of the eye. The incidence of diseases of the eye that require

surgical intervention in the US is rapidly increasing due to growth in the elderly population segment. The National Eye Institute estimates that by the age of 80, half of all Americans will have either have or have had cataract surgery [33]. Cataract surgery is a complex procedure, and many aspects of the surgery would benefit from an enhanced sense of touch. A *keratectomy* is an incision made from the side of the eye to access the lens, using a triangular blade. A *capsulorhexis* is then done, where a pick is used to access the lens through the capsule. A specialized instrument is then used to break up and vacuum away parts of the clouded lens using high-intensity ultrasonic vibrations, a process called *phacoemulsification*. Placing intraocular implants and suturing incisions then follows. At each step, enhanced haptic feedback could improve outcome and safety, because the size of the anterior chamber restricts movement, or tissue interactions must be carefully monitored to avoid damage. Even thicker tissues, like the sclera, which must be cut to access the interior of the chamber, rarely provide tactile sense to the operating physician.

It is estimated that in 2012, 13 million ophthalmic surgical procedures will be conducted in the US among the sub-specialties of (i) cataract surgery, (ii) refractive surgery, and (iii) vitrectomy. Our initial target applications for the HHFM, cataract surgery and vitrectomy, are estimated to have a combined reachable market size of \$8.7 Billion [34]. Cataract surgery alone is predicted to have a \$7.8 billion world market by 2015 [35]. The volume of vitrectomies and cataract procedures is projected to grow to 350,000 and 3,851,000, respectively, by 2015 [36]. The volume of these surgical procedures is expected to grow at an annual rate of 5%. Because no commercially available technology exists that attempts to solve the haptic problem in microsurgery, a future HHFM start-up company would be well-positioned to take first mover advantage.

5.2.2 Emergent Engineering Challenges

One key challenge facing adoption of the HHFM in the operating theatre is sterilizability. Here, modularity in the overall HHFM system will help ease constraints or provide potential alternative configurations of a final device. For example, a reusable actuator assembly not requiring sterilization could be attached inside a surgical glove, communicating with a disposable sterile tool handle and tip through the glove. The effect of sterilization on long-term device functionality will need to be carefully studied. Autoclaving, the standard sterilization method for traditional durable surgical instruments, may not be appropriate if the HHFM is constructed of lightweight plastic. Other sterilization methods, like ethylene oxide or ultraviolet light exposure, may be recommended instead. The electronics powering the HHFM will need to be specially designed to be used in the sterile operating theatre.

Modularity of the HHFM will also play an important role when considering large scale manufacturing and quality assessment. Each individual assembly of the Model-2 HHFM was constructed using well-established manufacturing and machining capabilities, and uses commercially available parts. Sensors, actuators, and all aspects of the electronics of the devices were chosen with particular attention to cost at high volumes. Simplicity of construction allows for automation of the manufacturing process, delivering tight tolerances and high throughput at a relatively low cost. Disposable products, made from plastics, could be very easily adopted for high volume manufacturing procedures.

However, system modularity can also be a disadvantage when producing a commercial product. Differing manufacturing processes, each with distinct reliability and performance characteristics, increase complexity of the manufacturing endeavor. Supply chain complexities may further complicate the manufacturing process, since the sensor or actuator assemblies may be comprised of multiple commercial parts. Tolerances will need to be carefully controlled to ensure individual components of the HHFM system connect correctly. Quality assurance endeavors will need to take all of this variability into consideration when determining the final specifications of a particular HHFM system.

As the design of the HHFM is further refined for use in the clinic, usability studies will need to be done to characterize long-term device reliability and possible failure modes. Instability due to mechanical feedback between sensor and actuator assemblies, especially a problem as gain is increased, will need to be eliminated. Braking systems will need to be integrated to reduce membrane piercing “skid”. In general, anterior segment surgeries require many different tools, so work will need to be done that investigates how to best integrate the HHFM into as many tools as possible without becoming a burden on the surgical team. A solution to this particular problem is proposed in *Section 5.2.4*.

5.2.3 Intellectual Property and Patent Landscape

Two provisional patents protecting the HHFM were filed on September 27, 2010 and June 9, 2011 by Professor George Stetten. The first academic paper regarding the HHFM was not published until June 22, 2011 at the Information Processing in Computer Aided Intervention (IPCAI) conference in Berlin, Germany. At IPCAI 2011, our submission was awarded “Best Poster.” Full US patent and PCT applications were filed September 27, 2011. All applications were through the University of Pittsburgh Office of Technology Management (OTM).

Claims in the HHFM patent applications are broad enough to protect many realizations of the HHFM concept, including catheter based devices and finger-tip mounted versions. Parts of the device that may be individually detachable and sterilizable are also protected in the patent application. In

January 2012, Frost and Sullivan was commissioned to conduct a preliminary patent landscape search. **Figure 5-2**, from the Frost and Sullivan report, shows the recent trends in patent publishing in the field of haptic feedback technology. However, no formal freedom to operate or patent landscape reviews have been performed to this date.

In March 2012, the HHFM was presented as a demonstration to the 2012 Haptics Symposium in Vancouver, British Columbia, where academic colleagues from around the world were able to use the HHFM. Industry presence at the conference was strong, and included corporate representatives from Intuitive Surgical, who had previously contacted Dr. Stetten directly to inquire about the technology.

In April 2012, the University of Pittsburgh Office of Enterprise Development (OED) submitted on behalf of MagniFeel an application to the LifeSciences Accelerator StartUp Program at the Idea Foundry, a technology incubator and venture capital firm based in Pittsburgh, PA. Funds from this program would be used to support intellectual property prosecution and additional market research.

Patent Publishing Trends

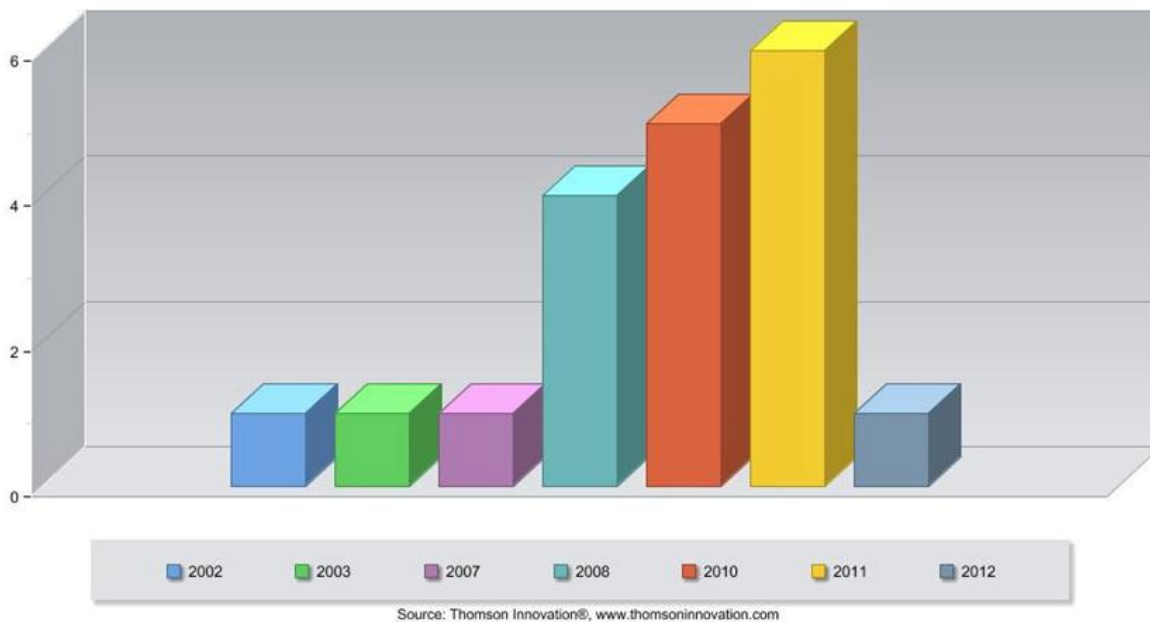


Figure 5-2. Patent publishing trends in haptic technology. Source: Frost & Sullivan report.

5.2.4 Proposed Business Model

The surgical instrument industry is one centered on technology. Surgical instruments are durable tools, and many clinicians have their own personal set, as familiar to them as a favorite ink pen or wrist-watch. These tools of the trade are chosen by surgeons chiefly on the basis of procedural need,

but variations may come down to personal preference. If the HHFM is to be adopted by clinicians as a trusted surgical tool, it is essential to prove that our tools will help where others have failed. But if a technology is too cumbersome, or conflicts too much with the existing infrastructure, adoption will be slow and painful. The practice of medicine has always been an exercise in controlled chaos, and care providers have been hard pressed to gamble away their time-tested experience for novel tools at every turn.

As a result, we recognize that in this competitive industry, the HHFM must be a product that improves patient outcomes, providing maximal benefit for its cost, and can also fit seamlessly into the existing paradigm. Surgeons have always been able to invent and adapt procedures to best take advantage of the tools at their disposal. With the advent of the HHFM, surgeons will be able to continue this process, refining their techniques in areas that have been excluded thus far.

If a new company is founded to produce the HHFM for clinical use, it will be subject to significant start-up research and development costs. Preliminary regulatory counsel has suggested that the HHFM should fall under a Class II classification, and should be approved for use through a 510(k) “substantial equivalence” pathway. While the clinical trial burden for Class II approval is significantly less extensive than a Class III investigational device, small usability trials may still be necessary. It is estimated that \$500,000 will be required to fund development of the HHFM until animal trials have been completed, at which point Series A funding amounting to \$4 million will be required to complete usability trials and finalize manufacturing and supply chain contracts.

However, upon entering the market, such a company would have a correspondingly large and well-established reimbursement pathway. For procedures requiring observation and recovery at a care facility, surgical tools are billed to third-party payers as a line item in the treatment for a diagnosis related group (DRG). In out-patient procedures, on the other hand, instruments are billed on a procedural basis, according to current procedural terminology (CPT) codes. There are well established DRG and CPT codes for anterior segment surgery of the eye. With help from the University of Pittsburgh OED, coordinators at the University of Pittsburgh Medical Center (UPMC) have been made available to consult on potential reimbursement schemes for the HHFM from the perspective of a large academic medical center.

As mentioned previously, most anterior segment surgeries require a variety of distinct tools. However, the HHFM Base Device, comprising the force sensor, device body, and force actuator, requires a solid connection to the user’s hand to transmit augmented forces, which renders switching between individual HHFM surgical tools inconvenient when multiple instruments are required. To address this

disconnect, we plan to design and produce a set of single-use tool tips that will interface directly to the HHFM Base Device. The tool tips will be modeled after common surgical tools—forceps, scrapers, and blades—but designed so that they may be easily exchanged during the procedure as needed. This approach has the distinct advantage of allowing a clinician to adapt procedures as appropriate, without restriction to any particular type of tool. Furthermore, high volume manufacturing of these tool tips will drive down costs, and the single use restriction will lead to high recurring profits. We estimate that each surgical tool tip set will cost \$20 to manufacture, and will be sold for approximately \$100.

The approach surrounding distribution of our HHFM Base Device is more flexible. A full determination can only be made when specifications of the final product have been determined. However, one option is to follow a “limited use” restriction for each device. This model is comparable to that of Intuitive Surgical and their *da Vinci* robot, where arms for the *da Vinci* are replaced every 10-15 procedures. This approach serves a two-fold purpose for our customer: first, to limit the stress from repeated sterilization and use, thus reducing the chance of failure, and second, to distribute costs of using the HHFM system over multiple procedures. The advantage of such an approach for the company is that it generates an additional stream of recurring revenue. Although manufacturing processes for the base HHFM will be necessarily more complicated than in the tool tip sets, we estimate that at high volumes, the base HHFM will cost approximately \$100 to manufacture, and can be sold for \$1000, to be used in 10 procedures.

To market the HHFM effectively, the device must be a presence at professional and societal meetings. As has been our experience with the initial HHFM prototypes, demonstrations are an essential way of publicizing our idea as a solution to the haptic problem in surgery. User studies and small clinical trials, whether or not they are required for regulatory approval, will also be an effective method of capturing the attention of initial clinical customers. Collaborating physicians, whether they are residents at an academic medical center or attending surgeons at a large county hospital, may become our first converts.

5.3 Conclusion

In this thesis, we have described the development of the Hand-Held Force Magnifier, a novel surgical tool that can augment a surgeon’s sense of touch during minimally invasive or microsurgical procedures. Although the first two prototypes of the HHFM worked well as proofs of concept, additional work is required if the HHFM is to ever see use as part of a surgical procedure. Psychophysical studies

are essential to fully understanding the limits and benefits of an augmented surgical tool. Collaboration with practicing surgeons will be essential in identifying the best way to safely and efficiently introduce the HHFM into the surgical toolkit. Because the HHFM does not currently have any direct competitors, the market is set to welcome a new device that can bring an additional layer of confidence to surgeons performing delicate operations.

References

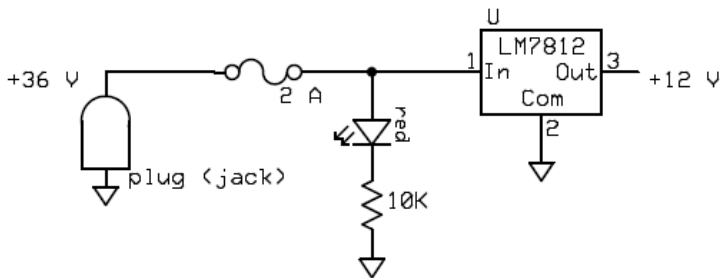
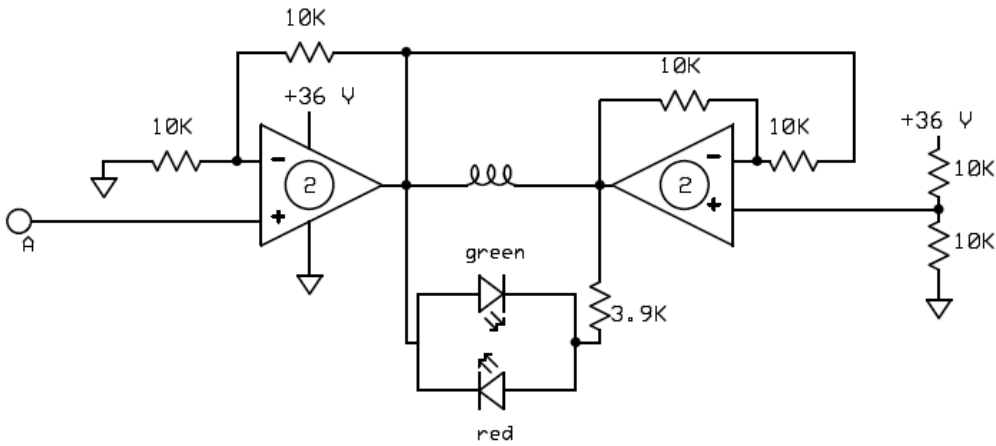
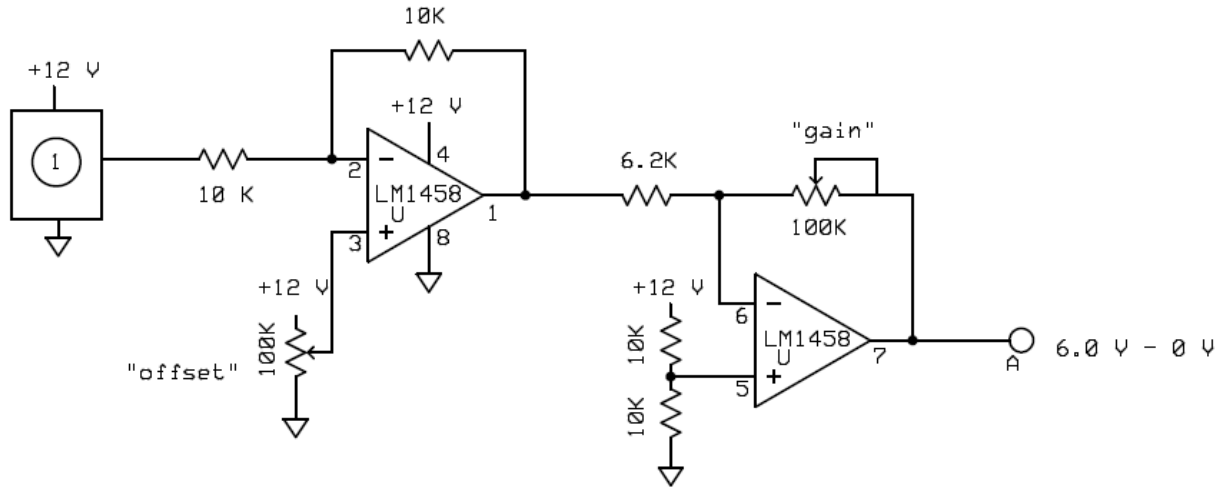
- [1] Rutkow, I. "History of Surgery." In: Sabiston Textbook of Surgery: The Biological Basis of Modern Surgical Practice, 19th edition, edited by C.M. Townsend, Jr., R.D. Bauchamp, B.M. Evers, K.L. Mattox. Philadelphia: Elsevier-Saunders, 2012.
- [2] Soper, N.J., L.M. Brunt, K. Kerbl. "Laparoscopic General Surgery." *NEJM*. 1994; 330(6):409-419.
- [3] Boni, L., A. Benevento, F. Rovera, G. Dionigi, M. Di Giuseppe, C. Bertoglio, R. Dionigi. "Infective Complications in Laparoscopic Surgery." *Surgical Infections*. 2006; 7(Suppl. 2): S-109-S-111.
- [4] Jonsson, B. and N. Zethraeus. "Costs and Benefits of Laparoscopic Surgery—A Review of the Literature." *Eur J Surg*. 2000; Suppl 585: 48-56.
- [5] Berggren, U., T. Gordh, D. Grama, U. Haglund, J. Rastad, D. Arvidsson. "Laparoscopic Versus Open Cholecystectomy: Hospitalization, Sick Leave, Analgesia and Trauma Responses." *Br J Surg*. 1994;81(9):1362-1365.
- [6] "Minimally Invasive Surgery / Endoscopic and Laparoscopic Surgery." Available online at: <http://www.beltina.org/health-dictionary/minimally-invasive-surgery-endoscopic-laparoscopic.html>. Accessed 24 April 2012.
- [7] Park, D.W., P.U. Dugel, J. Garda, J.O. Sipperley, A. Thach, S.R. Sneed, J. Blaisdell. "Macular Pucker Removal With and Without Internal Limiting Membrane Peeling: Pilot Study." *Ophthalmology*. 2003; 110(1):62-64.
- [8] Brooks, H.L., Jr. "Macular Hole Surgery With and Without Internal Limiting Membrane Peeling." *Ophthalmology*. 2000; 107(10): 1939-48.
- [9] Candiello, J., M. Balasubramani, E.M. Schreiber, G.J. Cole, U. Mayer, W. Halfter, H. Lin. "Biomechanical Properties of Native Basement Membranes." *FEBS Journal*. 2007; 274: 2897-2908.
- [10] Gupta, P.K., P.S. Jensen, E. de Juan, Jr.. "Surgical Forces and Tactile Perception during Retinal Microsurgery." *Med Image Comput Comput Assist Interv (MICCAI)*. 1999; Proceedings in LNCS 1679: 1218-1225.
- [11] Stetten, G., B. Wu, R. Klatzky, J. Galeotti, M. Siegel, R. Lee, R. Hollis. "Hand-Held Force Magnifier for Surgical Instruments." *2nd International Conference on Information Processing in Computer-Assisted Interventions (IPCAI)*, June 22-23, 2011. Berlin, Germany. Proceedings in LNCS 6689, pp. 90–100.
- [12] Fraden, J. Handbook of Modern Sensors, 4th ed. New York: Springer, 2010.
- [13] Webster, J.G. Medical Instrumentation: Application and Design, 3rd ed. New York: John Wiley & Sons. 1998.

- [14] "Squiggle Micro Motor Technology." New Scale Technologies. Available online at: http://newscaletech.com/squiggle_overview.html. Accessed 18 April 2012.
- [15] MachLachlan, R.A., B.C. Becker, J.C. Tabares, G.W. Podnar, L.A. Lobes, Jr., C.N. Riviere. "Micron: an Actively Stabilized Handheld Tool for Microsurgery." *IEEE Transactions on Robotics*. 2012; 28(1): 195-212.
- [16] Becker, B.C., R.A. MacLachlan, L.A. Lobes Jr., C.N. Riviere. "Vision-Based Retinal Membrane Peeling with a Handheld Robot." *IEEE International Conference on Robotics and Automation (ICRA 2012)*, in publication.
- [17] Becker, B.C., S. Voros, L.A. Lobes Jr., J.T. Handa, G.D. Hager, C.N. Riviere. "Retinal Vessel Cannulation with an Image-Guided Handheld Robot." *Proc of IEEE Engineering in Medicine and Biology Conference*. 2010; 5420-5423.
- [18] Yao, H.-Y., V. Hayward, R.E. Ellis. "A Tactile Enhancement Instrument for Minimally Invasive Surgery." *Computer Aided Surgery*. 2004; 10(4): 233-239.
- [19] Lederman, S.J. and R.L. Klatzky, "Chapter 10: Perceiving Texture through a Probe." In: *Touch in Virtual Environments*, edited by M. L. McLaughlin, J. Hespanha, and G. Sukhatme. Upper Saddle River, NY: Prentice Hall PTR, 2002. pp. 180–193.
- [20] Balicki, M., A. Uneri, I. Iordachita, J. Handa, P. Gelhbach, R. Taylor. "Micro-force Sensing in Robot Assisted Membrane Peeling for Vitreoretinal Surgery." *Med Image Comput Assist Interv (MICCAI)*. 2010; 13(Pt. 3): 303-310.
- [21] Uneri, A., M.A. Balicki, J. Handa, P. Gehlbach, R.H. Taylor, I. Iordachita. "New Steady-Hand Eye Robot with Micro-Force Sensing for Vitreoretinal Surgery." *Proc IEEE RAS EMBS Int Conf Biomed Robot Biomechatron*. 2010;(26-29): 814-819.
- [22] Berkelman, P.J., L.I. Whitcomb, R.H. Taylor, P. Jensen. "A Miniature Microsurgical Instrument Tip Force Sensor for Enhanced Force Feedback during Robot-Assisted Manipulation." *IEEE Transactions on Robotics and Automation*. 2003; 19(5): 917-922.
- [23] Sun, Z., M. Balicki, J. Kang, J. Handa, P. Gehlbach, R. Taylor, I. Iordachita. "A Sub-Millemetric, 0.25mN Resolution Fully Integrated Fiber-Optic Force Sensing Tool for Retinal Microsurgery." *Int J Comput Assist Radiol Surg*. 2009; 4(4): 383-390.
- [24] Culjat, M.O., C.-H. King, M.L. Franco, C.E. Lewis, J.W. Bisley, E.P. Dutson, W.S. Grundfest. "A Tactile Feedback System for Robotic Surgery." *Proc of IEEE Engineering in Medicine and Biology Conference*. Vancouver, Canada. August 20-24, 2008.
- [25] King, C.H., M.O. Culjat, M.L. Franco, J.W. Bisley, G.P. Carman, E.P. Duston, W.S. Grundfest, "A Multi-element Tactile Feedback System for Robot-Assisted Minimally Invasive Surgery," *IEEE Transactions on Haptics*. 2009; 2(1):52-56.

- [26] King, C.H., M.O. Culjat, M.L. Franco, J.W. Bisley, E. Dutson, W.S. Grundfest. "Optimization of a Pneumatic Balloon Tactile Display for Robot-Assisted Surgery Based on Human Perception." *IEEE Transactions on Biomed Eng.* 2008; 55(11):2593-2600.
- [27] RadioShack Part #640-1895 Specifications. Available online at: http://support.radioshack.com/support_supplies/doc19/19400.htm. Accessed 02 May 2012.
- [28] Berkelman, P. and R.L. Hollis. "Dynamic Performance of a Magnetic Levitation Haptic Device." *Proceedings of Conference on Telematipulation & Telepresence, SPIE Int'l Symposium on Intelligent Systems and Intelligent Manufacturing*. Greensburgh, PA. 1997; SPIE Proceedings Vol. 3602.
- [29] Butterfly Haptics, LLC. "Maglev 200 Magnetic Levitation Haptic Interface" Specification Sheet. Available online at: <http://butterflyhaptics.com/products/system/>. Accessed 04 May 2012.
- [30] Stevens, S.S. *Psychophysics: Introduction to its Perceptual, Neural, and Social Prospects*. New York: John Wiley. (1975).
- [31] Vokoun, D., M. Beleggia, L. Heller, P. Sittner. "Magnetostatic Interactions and Forces Between Cylindrical Permanent Magnets." *Journal of Magnetism and Magnetic Materials*. 2009; 321:3758-3763.
- [32] "SQL-3.4 Motor." New Scale Technologies. Available online at: <http://newscaletech.com/motorsforoem-SQL34.html>. Accessed 07 May 2012.
- [33] National Eye Institutes. "Facts about Cataracts." Available online at: http://www.nei.nih.gov/health/cataract/cataract_facts.asp. Accessed 29 April 2012.
- [34] "Global Ophthalmology Market (2009-2014)." Markets and Markets. <http://www.marketsandmarkets.com/Market-Reports/global-ophthalmology-devices-drugs-market-137.html>.
- [35] PRLOG: Press Release Distribution. "The Global Cataract Surgery Market was Valued to Reach \$7.8 Billion by 2015." Available online at: <http://www.prlog.org/10223650-the-global-cataract-surgery-market-was-valued-to-reach-78-billion-by-2015.html>. Accessed 29 April 2012.
- [36] Harmon, D. and J. Merritt. "Demand for Ophthalmic Services and Ophthalmologists – A Resource Assessment." Available online at: [http://www.meditec.zeiss.com/C1256CAC0038CEFF/EmbedTitelIntern/Market_Resource_White_Paper_04-2009/\\$File/Market_Resource_White_Paper_04-2009.pdf](http://www.meditec.zeiss.com/C1256CAC0038CEFF/EmbedTitelIntern/Market_Resource_White_Paper_04-2009/$File/Market_Resource_White_Paper_04-2009.pdf). Accessed 29 April 2012.
- [37] "Wheatstone bridge." Wikipedia. Accessed 09 May 2012.

Appendix A

Model-1 Electronics

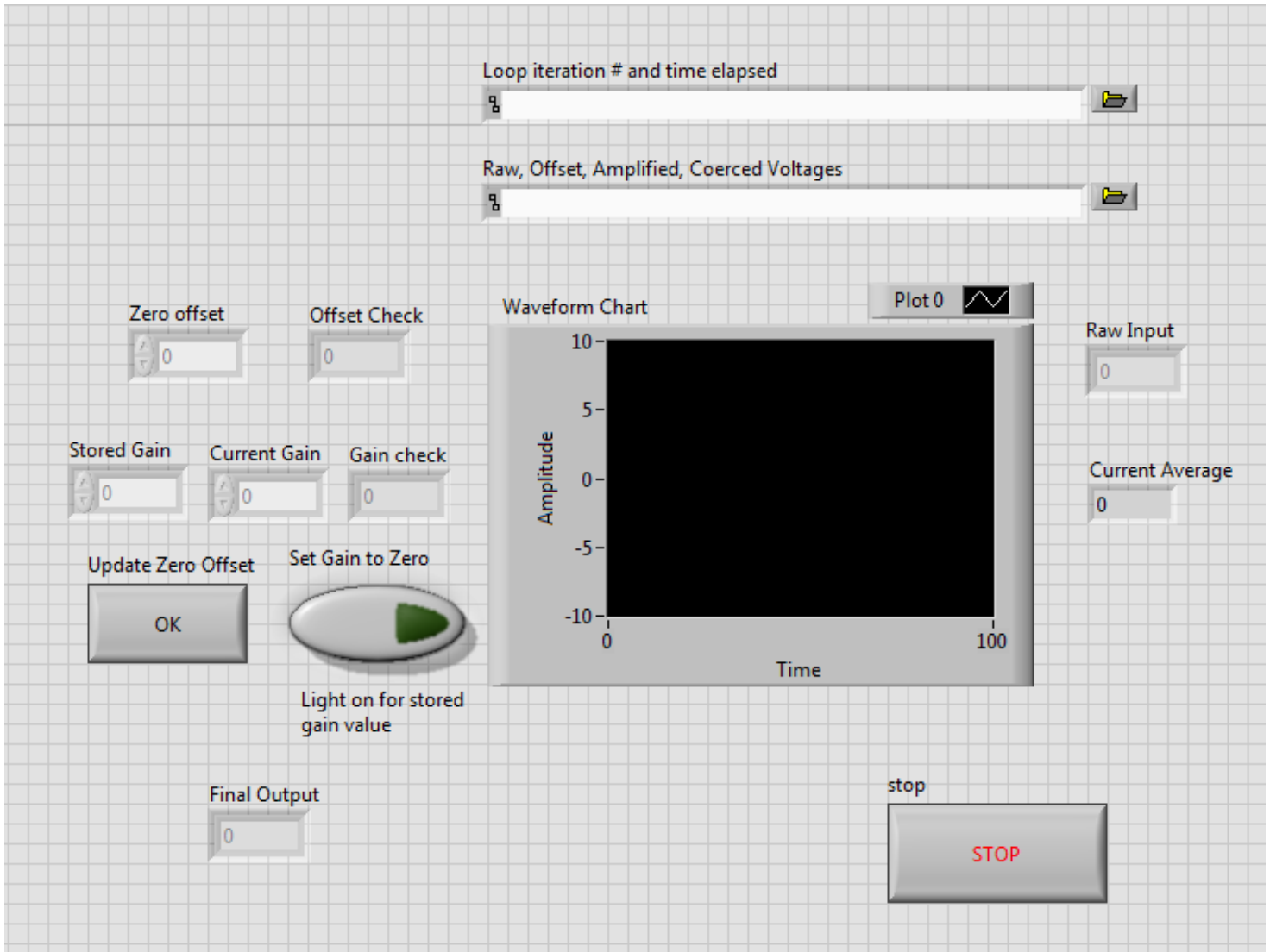


- ① Honeywell FS01 Force Sensor
- ② Apex PA74A

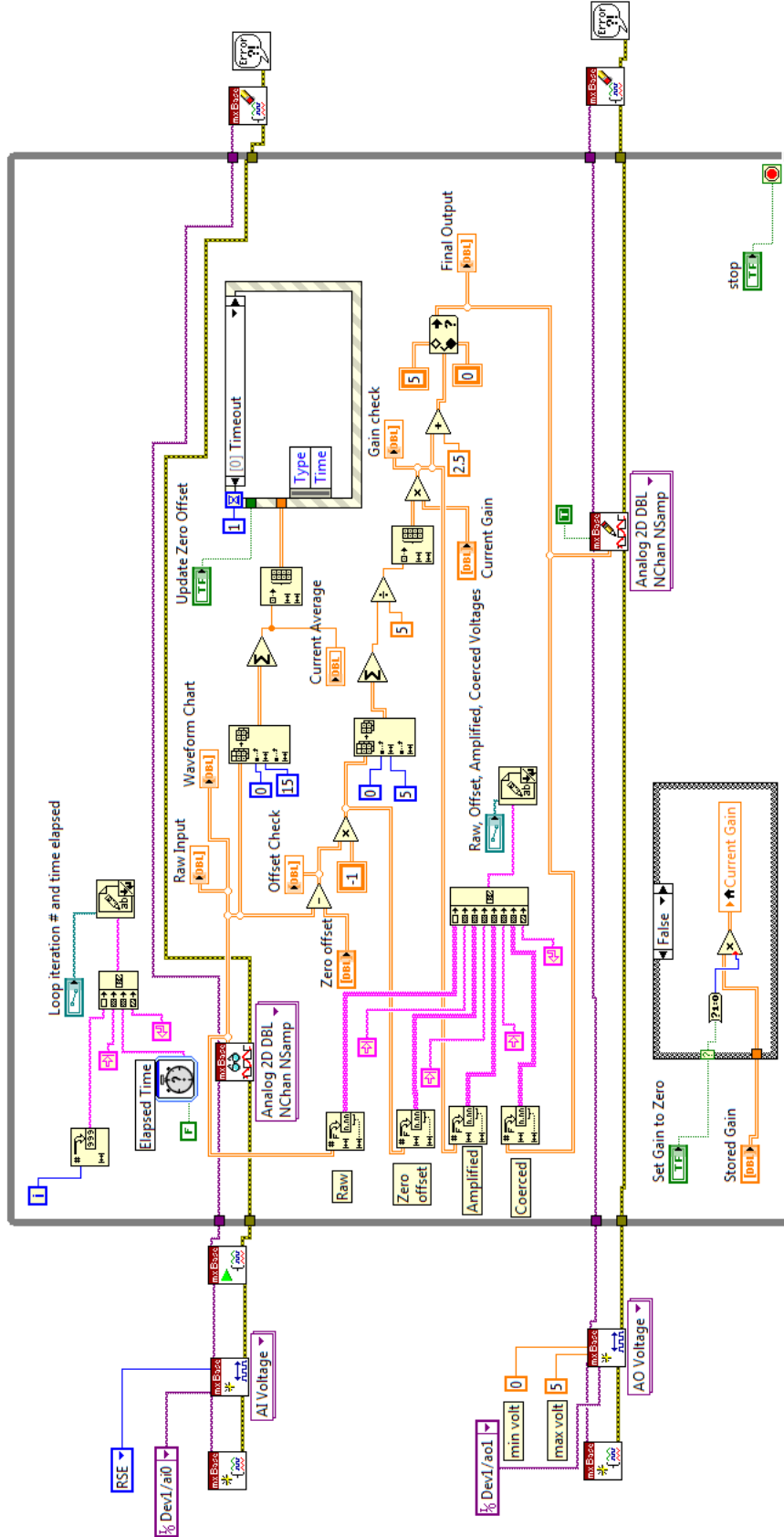
Appendix B

Model-2 Control Code (LabVIEW)

VI "Front Panel" (GUI)



VI "Back Panel"



Model-2 Control Code (Analog Devices)

```
/******
```

```
Randy Lee (randyl@andrew.cmu.edu)  
VIA Lab  
Carnegie Mellon University  
HHFM MCU Control
```

```
Analog Devices ADUC7026 hardware, HHFM Model-2 (Shim Stock Cage)
```

```
Code version: v015
```

```
Description and Notes:
```

```
Analog force measurement taken from ADC0 channel on range 0-2.5V.  
Signal subtracted from a constant which is calculated by taking  
the average of a randomly sampled signal over one second. Zero-centered  
signal obtained when device in use; multiplied by gain. Resultant DAC3  
output centered around 1.5V, with rails at 2.08V and 0.92V (max displacement  
from midpoint is 1.75/3 V).
```

```
v015-- Gain knob only set after tare button pressed  
v014-- Added potentiometer calculation of k_d to help tune PID position tare  
v013-- Added "mute" button functionality on P1.5  
        Fixed P1.1 tare routine to ensure sensor voltages obtained  
        Changed gain calculation to only occur when tare button pressed  
v012-- Implemented PD control for position tare  
v011-- Changed tare routine to "turn off" coil for 1 second and sample  
        Press button quickly to tare voltage, hold button to tare position  
v010-- Removed output "filter" and fixed ADC conversion routines  
v009-- Implemented PID control for position tare, generalized digital input  
        check function  
v008-- Implemented first order proportional control for position tare  
v007-- Removed PD control and implemented 5 measurement average "filter"  
v006-- Implement PD control with simple finite differentials  
v005-- Average sensor voltage calculation with pseudo-random sampling  
v004-- Timer working with IRQ structure  
v003-- Working timer sequence, need to fix period  
v002-- Adds variable gain functionality with potentiometer  
v001-- Introduces tare functionality with push button  
v000-- Simple implementation with hard-coded constants
```

```
Last Updated 22 March 2012
```

```
*****/
```

```
#include <aduc7026.h>
```

```
#include <math.h>
```

```
//#define TRUE 1;
```

```
//#define FALSE 0;
```

```
//#define GAIN 1;
```

```
//#define MIDPOINT 1.5;
```

```
unsigned int uiPLLTST = 0; // Unknown variables
```

```
volatile unsigned int ucTest = 0;
```

```
/* Variable Declarations */
```

```
int randomVoltageArrayCounter, randomWaitCounter, timeToWait;
```

```

int hardwareTimerDoneFlag = 0;
int randomSampleFlag = 0;

int randomDelayTimes[] = {132,163,186,124,177,7,91,112,122,102,145,63,
                        88,130,15,34,129,45,149,170,125,111,101,180,
                        153,140,53,125,171,166,36,57,68,128,72,95,140,
                        79,140,185,45,124,129,144,75,152,160,153,62,29,
                        1,40,133,157,84,68,139,157,24,192,12,178,24,92,
                        73,1,56,120,8,113,63,34,127,169,71,191,133,60,
                        139,193,141,139,184,51,167,154,175,80,176,123,
                        41,95,152,26,122,155,29,131,165,84};

// Set of 100 uniform from 1 to 200
// Average = 109.24
// Obtained 14 Feb 2012 @ 2:05pm from random.org/integers

float fullscale_gain = 60.00;
float midpoint = 1.50;
float sensor_voltage, transformed_voltage, offset_voltage, gain;
float storedRandomSamples[100];

/* Subfunction Definitions */
float ADCinput(int ADC_hex_result);
// converts hex ADC conversion result to workable decimal voltage
float calculatePOTvoltage(int hex_POT_voltage, float fullscale_value);
// converts voltage from potentiometer to a numerical gain
float calculateMeanFromStoredRandomSamples(void);
// offset_voltage update using mean of stored sensor voltages
int getSwitchSTATE(int port_number, int pin_number);
// fetches state from push switch on digital I/O port.pin
// pushed state returns 1
int outputDAC(float desired_voltage);
// converts desired decimal voltage to hex integer ready for DAC output
int waitForRestOfPeriod(void);
// uses hardware timer to wait until 100us period is over
// regulates 10kHz sampling rate

void ADCpoweron(int); // Initialize ADC
void timer_IRQ(void); // Interrupt routine for hardware timer
// sets timer expiration flag
void timer0Init(void); // Initialize timer0 routine
void delay(int); // Software delay

void storeSensorVoltageRandomly(void); // waits number of loops equal to element of
// randomDelayTimes to store sensor_voltage

void coilPositionTare(void); // Tare voice coil to correct position using
// PID while button remains pushed

int main(void)
{
    /* Core clock and power state control */
    POWKEY1 = 0x01;
    POWCON = 0x00; // Configures CPU Clock for 41.78MHz, CD=0
    POWKEY2 = 0xF4;

```

```

PLLKEY1 = 0xAA;
PLLCON = 0x01;
PLLKEY2 = 0x55;

/* Power on ADC and DAC channels, initialize digital I/O pins */
ADCpoweron(20000); // Power on ADC
REFCON = 0x01; // Connect internal 2.5V reference.
// 2.5V on Vref pin

DAC3CON = 0x12; // Set DAC3 output to 0-V_ref range
//and turn DAC3 on

GP1CON = 0x00; // Set digital I/O port 1 as general purpose
// I/O on pins .0-.7

GP1DAT = 0x00; // Set all I/O pins as input

/* Timer0 Set-up */
timer0Init(); // 100 us period, periodic countdown

IRQEN = 0x4; // Enable timer0 interrupt
IRQ = timer_IRQ; // Specify interrupt routine

/* Initialize necessary variables */
//offset_voltage = 1.70;

/* Initialize random time sampling routine*/
randomVoltageArrayCounter = 0;
randomWaitCounter = 0;
timeToWait = randomDelayTimes[0];

while(1)
{
    if(getSwitchSTATE(1,1) == 1) // Tare routine on P1.1 switch push
    {
        ADCCP = 0x05;
        ADCCON = 0x6A3;
        ADCCON &= ~(1 << 7);
        while(!ADCSTA){}
        gain = calculatePOTvoltage(ADCDAT, fullscale_gain);

        randomWaitCounter = 0;
        randomVoltageArrayCounter = 0;
        timeToWait = randomDelayTimes[0];
        randomSampleFlag = 0;
        while(randomSampleFlag == 0)
        {
            DAC3DAT = outputDAC(1.50);
            ADCCP = 0x00;
            ADCCON = 0x6A3;
            ADCCON &= ~(1 << 7);
        }
    }
}

```

```

        while (!ADCSTA){}
        sensor_voltage = ADCinput(ADCDAT);
        storeSensorVoltageRandomly();
        waitForRestOfPeriod();
    }
    offset_voltage = calculateMeanFromStoredRandomSamples();
    coilPositionTare();
}

if(getSwitchSTATE(1,2) == 1) // "Mute" routine for P1.5 switch
{
    while(getSwitchSTATE(1,2) == 1)
    {
        DAC3DAT = outputDAC(1.50);
    }
}

ADCCP = 0x00;
ADCCON = 0x6A3;
ADCCON &= ~(1 << 7);
while (!ADCSTA){}
sensor_voltage = ADCinput(ADCDAT);

transformed_voltage = (sensor_voltage - offset_voltage)*gain + midpoint;

DAC3DAT = outputDAC(transformed_voltage);

waitForRestOfPeriod();           // Hardware-timed wait to pace out sensor
                                // measurement at 10kHz (period = 100us)
}
}

void ADCpoweron(int time)
{
    ADCCON = 0x20;                // power-on the ADC
    delay(time);                  // wait for ADC to be fully powered on
}

void delay(int time)              // software delay. i = 10 --> ~12 us
{
    while (time >=0)
        time --;
}

void timer0Init()
{
    TOLD = 0x1000;                // 4096/ 41.86 MHz --> 100us
    TOCON = 0xC0;                 // enable timer0, set in periodic mode with multiplier = 1
}

void timer_IRQ()
{
    hardwareTimerDoneFlag = 1;
    TOCLR = 0xFF;                 // Clear interrupt
}

```

```

int getSwitchSTATE(int port_number, int pin_number)
{
    int pinInputData, pinInputData_MASKED, pinBit;

    if (port_number == 0){pinInputData = GP0DAT;}
    else if (port_number == 1){pinInputData = GP1DAT;}
    else if (port_number == 2){pinInputData = GP2DAT;}
    else if (port_number == 3){pinInputData = GP3DAT;}
    else if (port_number == 4){pinInputData = GP4DAT;}

    pinBit = pow(2,pin_number);
    pinInputData_MASKED = (pinInputData & pinBit); // Masked result shows only
                                                    // bit corresponding to pin number

    if (pinInputData_MASKED == 0)                // bit is LOW when pushed, HIGH when not
        {
            return(1);
        }
    else
        {
            return(0);
        }
}

float ADCinput(int ADC_hex_result)
{
    float input_voltage;
    int ADC_hex_result_shifted;
    ADC_hex_result_shifted = ADC_hex_result >> 16;
    input_voltage = ((ADC_hex_result_shifted)*2.52)/(0xFFFF);
                    // 2.52 chosen experimentally with ADC connected to voltmeter
    return(input_voltage);
}

int outputDAC(float desired_voltage)
{
    int output_integer = floor((desired_voltage*0xFFFF)/2.497);
                    // "unit conversion" from desired decimal voltage to hex code
                    // 2.4976 is voltage when 0xFFFF applied to DAC

    if (output_integer <= 0xFFFF && output_integer >= 0x200)
        output_integer = (output_integer - 0x2) << 16;
        // shift integer result 16 bits to left to conform to DACxDAT format

    // maximum and minimum integer cap
    // result subtracted from small integer as rough calibration to measured values
    else if (output_integer > 0xFFFF)
    {
        output_integer = 0xFFFF;
        output_integer = output_integer << 16;
    }
    else
    {
        output_integer = 0x200;
        output_integer = output_integer << 16;
    }
}

```

```

    }
    return(output_integer);
}

int waitForRestOfPeriod(void)
{
    if (hardwareTimerDoneFlag == 1)
    {
        hardwareTimerDoneFlag = 0;           // Reset timer flag
        return(0);
    }
    else
    {
        while(hardwareTimerDoneFlag == 0){} // Wait until interrupt request
        hardwareTimerDoneFlag = 0;
        return(1);
    }
}

float calculatePOTvoltage(int POT_voltage, float fullscale_value)
{
    float calculatedVoltage;
    int POT_voltage_shifted = POT_voltage >> 16;
    calculatedVoltage = (POT_voltage_shifted / (float) 0xFFF) * (fullscale_value);
    return(calculatedVoltage);
}

float calculateMeanFromStoredRandomSamples(void)
{
    int i;
    float sum = 0.0;
    float mean = 0.0;
    for(i = 0; i < 100; i++)
    {
        sum += storedRandomSamples[i];
    }
    mean = sum/100.0;
    return(mean);
}

void storeSensorVoltageRandomly(void)
{
    if (randomWaitCounter >= timeToWait)
    {
        storedRandomSamples[randomVoltageArrayCounter] = sensor_voltage;
        randomWaitCounter = 0;
        randomVoltageArrayCounter++;
        // Advance to next element in randomDelayTimes and storedRandomSamples arrays
        if (randomVoltageArrayCounter >= 100)

        {
            randomVoltageArrayCounter = 0;
            // Loop around random voltage array
            randomSampleFlag = 1;
            // Flag to signify all 100 samples taken
        }
    }
}

```

```

        timeToWait = randomDelayTimes[randomVoltageArrayCounter];
// Load next time to wait from randomDelayTimes array
    }
else
{
    randomWaitCounter++;
}
}

void coilPositionTare(void)
{
    float positionVoltageGoal = 1.0;
    float k_p = 0.75;
    float k_d;
    float fullscaleK_d = 10.00;
// float k_i = 0.2;

    float positionSensorVoltage, error, voltageToCoil;
    float errorDerivative, previousError;
// float errorIntegral;
// int errorArrayCounter=0;

    while(getSwitchSTATE(1,1) == 1)
    {
        /*
        ADCCP = 0x07;                                ADCCON = 0x6A3;
        ADCCON &= ~(1<<7);
        while(!ADCSTA){}
        k_d = calculatePOTvoltage(ADCDAT, fullscaleK_d);
        */
        k_d = -0.75;

        ADCCP = 0x06;                                // select ADC channel 6 reluctance sensor voltage
        ADCCON = 0x6A3;
        ADCCON &= ~(1 << 7);    // clear bit 7 to stop reluctance sensor conversion
        while(!ADCSTA){}
        positionSensorVoltage = ADCinput(ADCDAT);

        error = positionVoltageGoal - positionSensorVoltage;
            // Negative error means coil too close to cup, push out
            // Positive error means coil is past goal, pull back in

        //storedErrorCalculations[errorArrayCounter] = error;

        //Error Derivative
        errorDerivative = previousError - error;

        /*
        // Error Integral
        for(errorArrayCounter = 0; errorArrayCounter<5; errorArrayCounter++)
        {
            errorIntegral += storedErrorCalculations[errorArrayCounter];
        }
        errorArrayCounter++;
        if (errorArrayCounter>=5){errorArrayCounter = 0;}
        */
    }
}

```

```
voltageToCoil = 1.5 + (k_p * error) + (k_d * errorDerivative);  
DAC3DAT = outputDAC(voltageToCoil);
```

```
previousError = error;
```

```
}
```

```
}
```

